Deanticoagulated Heparins Mediate Goblet Cell Differentiation to Restore Mucosal Barrier for Ulcerative Colitis Therapy

Wei Hu[1, #], Zhen Kang Liu[1, #], Long Huang[1,2, #], Wen Zeng[2], Xiao Yi Ren[1], Yang Ji[3], Qin Xuan Zhou[1], Bing Xu[1,4], Can Yang Zhang[1,2,5,6], Chong Zhang[2,6], Zhen Qing Zhang[7], Hong Chao Zhang[8], Yun Sheng Yang[9], Ye Chen[10], Xuan Jiang[11, *], Yi Wang[2, *], Xin-Hui Xing[1,2,4,5, 6, *]

[1]Institute of Biopharmaceutical and Health Engineering, Shenzhen International Graduate School, Tsinghua University, Shenzhen 518055, China

[2]Key Laboratory for Industrial Biocatalysis, Ministry of Education, Institute of Biochemical Engineering, Department of Chemical Engineering, Tsinghua University, Beijing 100084, China

[3]School of Medicine, Southern University of Science and Technology, Shenzhen, Guangdong Province 518112, China

[4]Institute of Biomedical Health Technology and Engineering, Shenzhen Bay Laboratory, Shenzhen 518118, China

[5]Key Laboratory of Active Proteins and Peptides Green Biomanufacturing of Guangdong Higher Education Institutes，Tsinghua Shenzhen International Graduate School, Shenzhen 518055, China

[6]Center for Synthetic and Systems Biology, Tsinghua University, Beijing 100084, China

[7]Jiangsu Key Laboratory of Translational Research and Therapy for Neuro-Psycho-Diseases and College of Pharmaceutical Sciences, Soochow University, Suzhou, Jiangsu 215021, China

21 [8]Department of Cardiovascular Surgery, Air Force Medical Center, Beijing 100142, China

22 [9]Department of Gastroenterology and Hepatology, Chinese PLA General Hospital, Beijing

23 100853, China

24 [10]Department of Gastroenterology, Southern Medical University Shenzhen Hospital,

25 Shenzhen 518101, China

26 [11]Department of Gastroenterology, Beijing Tsinghua Changgung Hospital, Beijing 102218,

27 China

28

Abstract

Impaired mucosal barrier function is a pathological hallmark of ulcerative colitis (UC), yet current clinical therapeutic strategies primarily rely on anti-inflammatory agents or surgery, lacking strategies to repair mucosal damage[1,2]. Here, through a systematic screen of our established library of deanticoagulated heparins[3], we found that the nonanticoagulant low-molecular-weight heparin NALHP (average Mw, 6400 Da; PDI=2.23) and its separated representative fine fragment S6 (average Mw, 4200 Da; PDI=1.1) significantly ameliorated dextran sulfate sodium (DSS)-induced UC in mice by restoring intestinal integrity. Both compounds promoted crypt stem cell differentiation into goblet cells, thereby repairing the colonic mucosal barrier. Notably, in human UC patient-derived organoids, NALHP and S6 enhanced goblet cell differentiation, increased MUC2 secretion, and modulated Wnt and Notch signaling to optimize epithelial composition. Our study is the first to reveal the therapeutic mechanism of deanticoagulated heparin derivatives in UC through the regulation of epithelial mucosal regeneration via the mediation of goblet cell differentiation, providing crucial insights for the development of novel UC therapeutics capable of targeting the mucosal barrier repair process.

46 **Introduction**

47 Ulcerative colitis (UC) is a chronic, idiopathic, and intractable disease that recurrently and
48 continuously triggers inflammation of the colonic epithelial mucosa[4-6] and is among the principal
49 inflammatory bowel diseases. Clinically, UC patients frequently exhibit symptoms such as
50 abdominal pain, loose stools, abscesses and bloody stools, low-grade fever, and malnutrition[5,7],
51 which can render them completely incapable of working and, further, potentially induce colon
52 cancer[8,9]. Although more than 160 years have passed since the first case of UC was reported in
53 the literature, there is still no clear and unified pathogenetic mechanism of UC. This lack is
54 attributed mainly to the complex pathogenesis and influencing factors of UC. It is generally
55 acknowledged that immunity, genes, the environment, and the gut microbiota are the four major
56 factors influencing the incidence of UC and that these four factors interact and jointly facilitate
57 the progression of UC. The complex and unknown pathogenesis of UC also poses difficulties and
58 challenges for drug development and clinical treatment. However, the main pathological feature
59 of UC at the endoscopic and molecular levels is substantial intestinal barrier damage, including
60 damage to the intestinal epithelial barrier and the mucous layer barrier, at the site of ulceration[2].
61 This feature is an important clinical hallmark indicating the efficacy of UC treatment[1]. However,
62 currently, the clinical treatment of UC mainly encompasses anti-inflammatory drug therapy
63 and/or surgical treatment[10]. Moreover, none of the existing treatments can completely cure UC.
64 More specifically, no treatment method can achieve complete tissue healing in the mucosal
65 layers of UC patients[2]. Given that there is currently no specific drug for UC treatment, drug

66 therapy regimens for UC generally consist of broad-spectrum anti-inflammatory drugs such as
67 nonsteroidal anti-inflammatory drugs, corticosteroids, immunosuppressants, and biologics[11].
68 Among these drugs, 5-aminosalicylic acid (5-ASA) drugs (mesalamine and olsalazine) are the
69 most widely utilized first-line clinical drugs for the anti-inflammatory treatment of UC[12]; these
70 drugs can begin to have effects within 2 to 4 weeks and alleviate the condition in approximately
71 53% of patients[13]. UC patients treated with corticosteroids (prednisone and budesonide), the
72 second-line drugs for UC treatment, have a remission rate of approximately 50%[14]; these drugs
73 are typically employed as a fallback option when 5-ASA treatment is ineffective. Biologics
74 (infliximab and adalimumab) are utilized for the treatment of patients with moderate to severe
75 UC and can directly act on inflammatory signaling pathways such as the tumor necrosis factor
76 alpha (TNF-α) and Janus kinase (JAK) pathways[15]. However, biologics are relatively costly, and
77 fewer than 30% of UC patients respond to biologic therapy[16]. Additionally, most of the new UC
78 drugs under development are biologics that act mainly on JAK, Sphingosine-1-Phosphate
79 Receptor 1 (S1P1), α4β7 integrin and other mediators to regulate immunity and inflammation[17].
80 However, these new drugs are unable to overcome the limitation of the 20% to 30% remission
81 rate of UC patients treated with biologics[2].
82 Heparin (HP) is a high-molecular-weight linear polysaccharide[18] with a complex molecular
83 structure characterized by an intricate sugar chain framework comprising alternating
84 glucosamine (GlcN) and hexuronic acid (HexA)—namely, glucuronic acid (GlcA) or iduronic
85 acid (IdoA)—units linked through α(1→4) or β(1→4) glycosidic bonds with elaborate acetyl and

86 sulfonic acid group modifications[19]. Owing to its highly sulfonated nature along with its intricate
87 sugar chain architecture[20], HP exhibits binding affinity for numerous proteins, leading to diverse
88 biological activities encompassing anticoagulant and other activities that have led to its clinical
89 application for more than 80 years[21], such as anti-inflammatory[22], antitumor[23], and antiviral[24]
90 activities. While the anticoagulant function of HP arises from specific pentasaccharide sequences
91 (GlcNS6S/GlcNAc6S-GlcA-GlcNS6S3S-IdoA2S-GlcNS6S) within its sugar chains that interact
92 with antithrombin III (ATIII), these sequences account for only approximately 30% of its
93 content, leaving much unexplored territory awaiting further investigation[20], and elucidating the
94 nonanticoagulant functions of HP remains pivotal in current academic research and the
95 development of next-generation HP drugs. A profound challenge in glycoscience is posed by the
96 structural complexity resulting from the presence of diverse monosaccharides and their
97 modifications, which form repetitive disaccharide units and complicate both structural and
98 functional analyses.
99 Gaffney *et al.*[25] fortuitously discovered in 1995 that the combination of subcutaneous
100 anticoagulant HP drug injection and oral sulfasalazine administration in 10 patients with UC
101 refractory to traditional drug therapy alleviated the disease in 9 of the patients, thereby initiating
102 anticoagulant therapy with HP for UC[26]. However, studies on anticoagulant HP drug therapy for
103 UC often have limitations, such as inconsistent conclusions[27-29], a lack of clarity regarding the
104 effective molecular structure, unknown mechanisms of action and a high risk of massive
105 bleeding in UC lesions because of the anticoagulant activity[30], indicating that clinical HP drugs

106 with anticoagulant activity cannot be effective for the treatment of UC. However, the well-
107 known nonanticoagulant activity of low-molecular-weight HP, with its specific targeting of
108 integrin αM–mediated immune cells at inflammatory sites, has been successfully used to develop
109 oral bifunctional nanotherapeutics that treat UC by ameliorating oxidative stress and inhibiting
110 the activation of inflammation-associated signaling pathways[29]. To address the problems of the
111 instability of anticoagulant HP drugs and the bleeding risk associated with their use in the
112 treatment of UC, in this paper, the deanticoagulated HP derivative library constructed by our
113 group[3] was used for in vitro and in vivo screening of anti-UC activity, and NALHP, a
114 nonanticoagulant low-molecular-weight HP with significant and stable treatment efficacy for
115 UC, as determined by oral administration to mice with DSS-induced UC, was discovered.
116 Through discriminative analysis, we discovered that NALHP, with an average molecular weight
117 (Mw) of 6400 Da and a polydispersity index (PDI) of 2.23, and its representative fine fragment
118 S6 separated by gel chromatography, with an average Mw of 4200 Da and a polydispersity index
119 (PDI) of 1.1 and accounting for 15.3% (w/w) of the content of NALHP, which was the highest
120 among the fragments, can be effectively used to treat UC in mice. Notably, the effective
121 deanticoagulated HP derivatives significantly restored the colonic mucosal barrier in UC model
122 mice by restoring the proliferation and differentiation ability of colonic crypt stem cells.
123 Furthermore, using human UC patient-derived colon organoids, we elucidated the detailed
124 mechanism through which NALHP and S6 increase the proportion of functional cells, especially
125 goblet cells, in the organoids by simultaneously inhibiting the activity of the Wnt and Notch

126 signaling pathways to promote the differentiation of intestinal stem cells into goblet cells,

127 thereby profoundly restoring the mucosal barrier.

128

129 **Results**

130

131 ***Deanticoagulated HPs: structural characterization***

132 In clinical practice, the manufacturing process of anticoagulant HP drugs primarily aims to

133 preserve the structural integrity of the anticoagulant pentasaccharide sequence. However, the

134 enrichment of sequences with anticoagulant activity during production may disrupt or impair the

135 more abundant nonanticoagulant sequences of HP molecules, thereby reducing the stability and

136 reproducibility of their nonanticoagulant therapeutic efficacy in ulcerative colitis (UC). To more

137 effectively investigate the consistent nonanticoagulant biological activity of HP, we previously

138 established a library of different structurally modified deanticoagulated HP derivatives, including

139 NAHP, I-45, NAI45, III,II-2-Odes, Eno (enoxaparin) and NAEno (nonanticoagulant enoxaparin)[3]

140 (Fig. 1a). Using the well-established mouse model of 3% dextran sulfate sodium (DSS)-induced

141 UC (Extended Data Fig. 1a), we evaluated the therapeutic efficacy of various modified

142 deanticoagulated HP derivatives in this library. As shown in Extended Data Fig. 1,

143 deanticoagulated HP (NAHP; average Mw, 13444 Da; PDI=1.28), an HP derivative obtained

144 through periodate oxidation followed by sodium borohydride reduction of heparin (HP; average

145 Mw, 17928 Da; PDI=1.28), in which the glucuronic acid of the pentasaccharide unit was ring-

opened, resulting in the loss of anticoagulant activity (Fig. 1a), exhibited stable efficacy in partially restoring the structure of the colon tissue (Extended Data Fig. 1b-g). However, the anticoagulant HP and the other four deanticoagulated HP derivatives prepared differently did not have this stable biological effect.

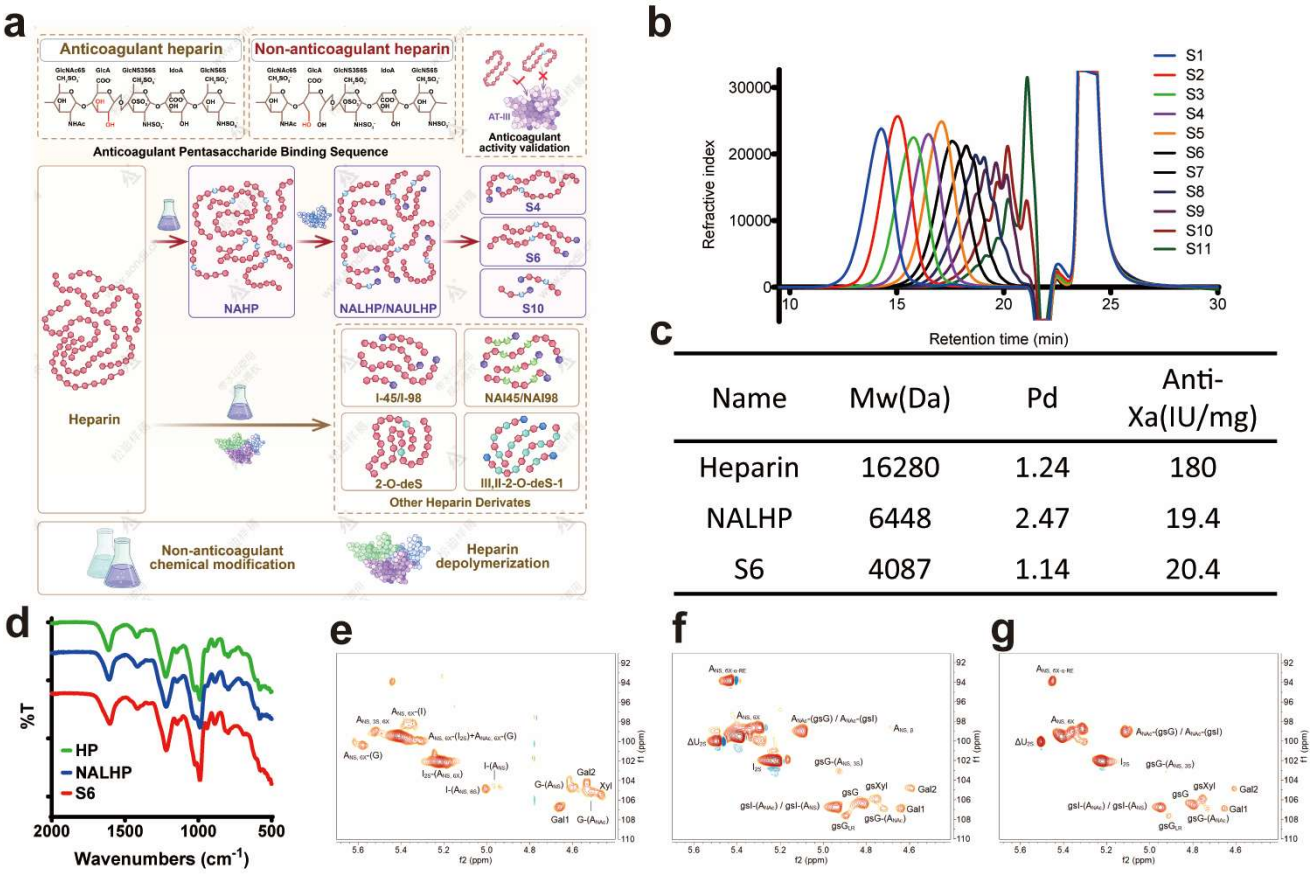

Name	Mw(Da)	Pd	Anti-Xa(IU/mg)
Heparin	16280	1.24	180
NALHP	6448	2.47	19.4
S6	4087	1.14	20.4

Fig. 1 Characterization of deanticoagulated HP derivatives. a, A library of deanticoagulated HP derivatives was constructed: NAHP (deanticoagulated HP, prepared by opening the structure of heparin with sodium periodate), I-45 (prepared by enzymatic hydrolysis with heparinase I until the absorbance increased to 45), NAI45 (opening the structure of I-45 with sodium periodate), III,II-2 (prepared by combined enzymatic hydrolysis with heparinase III and

156 heparinase II), Eno (enoxaparin) and NAEno (prepared by opening the structure of enoxaparin
157 with sodium periodate)[3]. **b,** Molecular weight HPLC chromatograms of S1-S11. **c,**
158 Physicochemical properties of HP and HP derivatives. **d,** Infrared spectra of HP and HP
159 derivatives. **e–g,** HSQC spectra of HP **(e)** and its derivatives NALHP **(f)** and S6 **(g)**.
160 Furthermore, compared with the first-line clinical drug 5-ASA, the respective nonanticoagulant
161 low-molecular-weight and ultra-low-molecular-weight HP derivatives of NAHP, i.e., NALHP
162 (average Mw, 6400 Da; PDI=2.33) and NAULHP (average Mw, 3800 Da; PDI=4.15), which
163 were obtained via controlled enzymatic hydrolysis of NAHP with heparinase I (Fig. 1a),
164 demonstrated even more pronounced therapeutic efficacy in UC model mice (Extended Data Fig.
165 2a-h). Both NALHP and NAULHP significantly ameliorated DSS-induced damage to the colonic
166 mucosal barrier and facilitated the restoration of intestinal crypt architecture (Extended Data Fig.
167 2a-h). They also effectively reduced the serum concentrations of inflammatory cytokines (IL-6
168 and TNF-α) by more than 50% (Extended Data Fig. 2g and h). Notably, compared with
169 NAULHP, NALHP, which can be prepared in a stable form by the established production process
170 (Extended Data Fig. 3a-d and Extended Data Tables 2-4), showed greater efficacy in decreasing
171 DSS-induced mortality (Extended Data Fig. 2i). Therefore, NALHP was selected for all
172 subsequent investigations. In addition, we found that the adsorption and desorption curves of
173 DSS and HP, NAHP, NALHP, and NAULHP were consistent with those of the water control
174 group by the biofilm layer interference technique, confirming that there was no interaction
175 between HP derivatives and DSS (Extended Data Fig. 2j and k).

176 Given the large difference in molecular weight between the enzymatic hydrolysis product
177 NALHP from NAHP (PDI=2.23 for NALHP vs. PDI=1.28 for NAHP), we performed fine
178 separation of NALHP using gel exclusion chromatography, collecting key fragments with an
179 average molecular weight difference of approximately 500 Da. A total of 11 distinct fractions
180 were obtained and designated S1 to S11 (Fig. 1a, b and Extended Data Table 1). Among these 11
181 separated fractions, S6, the intermediate-molecular-weight fraction of NALHP (Extended Data
182 Table 1, Extended Data Fig. 4c and d), with an average molecular weight of 4200 ± 150 Da
183 (PDI=1.1), exhibited bioactivity similar to that of NALHP (Fig. 1c and Extended Data Fig. 4). In
184 addition, S10 (average Mw, 1282Da; PDI=1.15) has no efficacy on mucosal remodeling. The
185 efficacy of NAULHP and S4 (average Mw, 6254Da; PDI=1.05) is inferior to that of NALHP and
186 S6. Structural characterization confirmed that S4 and S6 fully retained the characteristic
187 functional groups and sugar chain structure of the parent NALHP and NAULHP (Fig. 1d-g,
188 Extended Data Fig.9), but the main molecular structure of S10 is ΔHexA2S and the reducing end
189 is α-GlcNS6X, the Gal1, Gal2, Xyl and $GlcA_{LR}$ signal peaks in the LR region are missing
190 (Extended Data Fig.9). The above results together with the PCA of the UC treatment phenotypes
191 for HP, NAHP, NALHP, NAULHP, S4, S6 and S10 (Extended Data Fig.4j) indicate that in the
192 NALHP, the fragments with molecular weights ranging from 3000Da to 8000Da are the main
193 active components, and S6 is the representative fraction of NALHP with the similar biological
194 activity.
195 This consistent therapeutic efficacy is markedly distinct from that of native HP. Consequently,

196 we conducted a comparative structural analysis of UC-effective NALHP and S6 and UC-
197 ineffective native HP, NAI45 and other HP derivatives using Fourier transform infrared
198 spectroscopy (FTIR) and two-dimensional nuclear magnetic resonance spectroscopy (2D-NMR).
199 The results indicated that (1) the chemical modifications did not significantly alter the
200 characteristic functional groups of the HP polysaccharide chain, such as the N-sulfate and O-
201 sulfate groups (Fig. 1d and Extended Data Fig. 6); and (2) enzymatic hydrolysis specifically
202 introduced novel structural units—ring-opened glucuronic acid (gsGlcA) and Δ4,5-unsaturated
203 glucuronic acid—without inducing extensive structural modifications to the monosaccharide
204 units (Fig. 1e, f, Extended Data Figs. 7-9, Extended Data Tables 5 and 6).
205
206 ***Deanticoagulated HPs relieve UC pathology via mucosal repair***
207 The results obtained in the DSS-induced mouse model of colitis demonstrated that both NALHP
208 and S6 significantly improved the pathological phenotypes of DSS-induced UC in mice (Fig.
209 2a). Specifically, they effectively inhibited weight loss (Fig. 2b), restored the colon length to
210 92% of that in the normal group (Fig. 2c and e), and reduced the abnormal increase in the spleen
211 index by 40% (Fig. 2d and f). Furthermore, both NALHP and S6 significantly suppressed the
212 increase in the serum concentrations of IL-6 and TNF-α, decreasing the final concentrations by
213 62% and 90%, respectively (Fig. 2g and h). Histopathological analysis revealed that the colonic
214 crypt structure in the NALHP and S6 treatment groups was completely reconstructed (Fig. 2i4, i5
215 and j) and that the goblet cell density was restored to more than 85% of that observed in the

normal group (Fig. 2k4, k5 and l). These effects were significantly greater than those observed in the HP treatment group (Fig. 2i3, k3 and j) and the positive control drug (5-ASA) group ($p < 0.01$) (Fig. 2i6 and k6). The combined results of glycoprotein staining with WGA, EdU incorporation, and MUC2 immunohistochemical staining revealed marked restoration of the colonic mucus layer in the NALHP and S6 groups (Fig. 2 m4 and m5), whereas no such restoration was observed in the HP groups (Fig. 2m2 and m3). Slight restoration of the mucus layer was observed in the 5-ASA group (Fig. 2m6), but the degree of restoration was much lower than that observed in the NALHP and S6 groups. Additionally, the expression level of the mucin MUC2 in the NALHP and S6 groups was significantly greater than that in the model group ($p < 0.001$) (Fig. 2l). EdU incorporation assay results further confirmed that the intestinal epithelial cell proliferation index was significantly greater in the treatment groups than in the model group ($p < 0.001$) (Fig. 2n), whereas traditional drugs such as anticoagulant HP and the anti-inflammatory drug 5-ASA had no significant reparative effects. Collectively, these findings indicate that treatment with either NALHP or S6 can effectively repair mucosal injury in mice with DSS-induced colitis, restore colonic mucosal protein expression, and reconstruct the mucosal barrier.

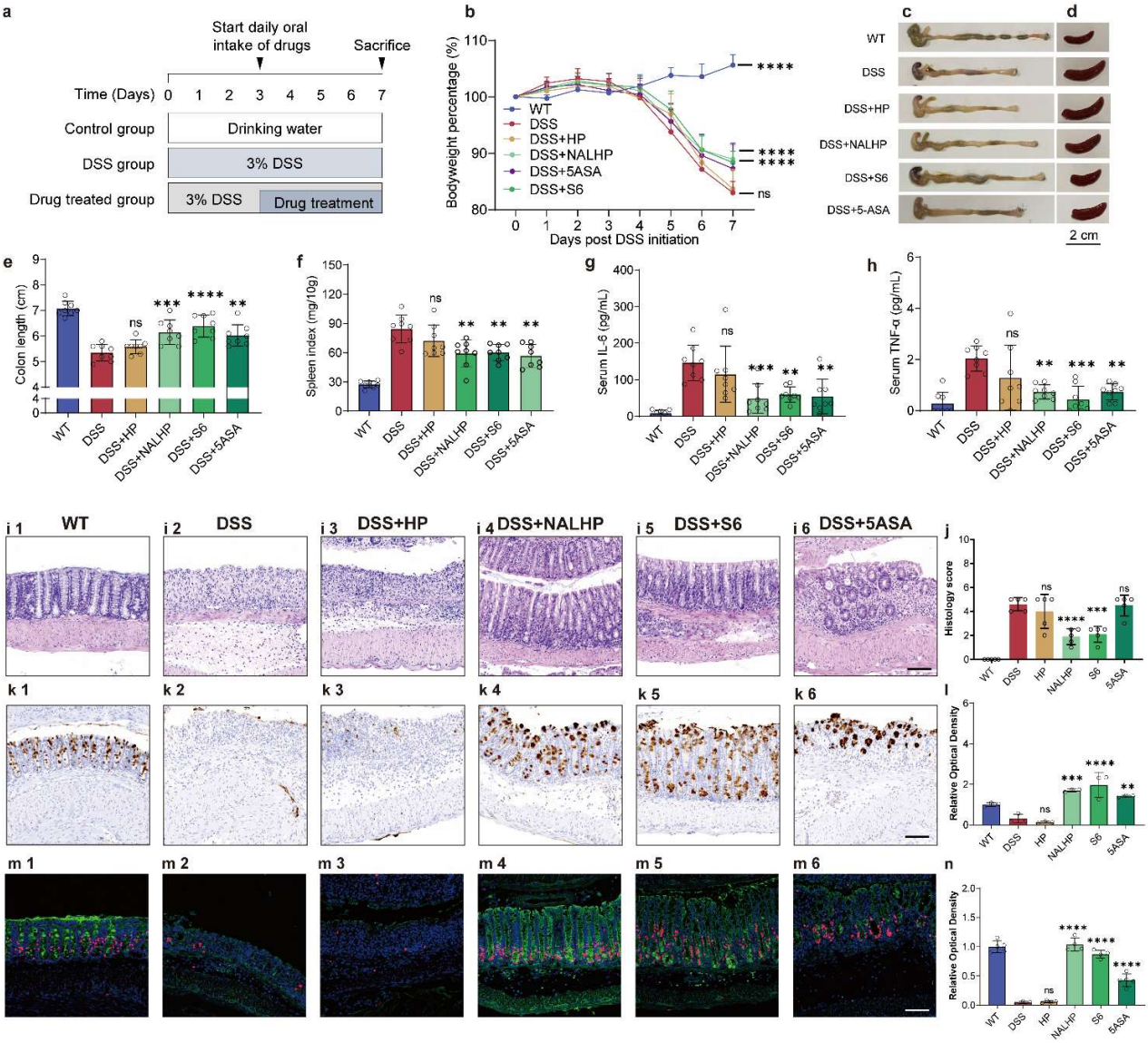

Fig. 2 Evaluation of the therapeutic efficacy of deanticoagulated HP derivatives. a, 3% DSS was added to the drinking water for 7 days to induce acute colitis in mice (n=8). The mice in the control group were given regular drinking water (n=8), and the mice in the drug treatment group were given 30 mg/kg HP, NALHP, S6, or 5-ASA on the third day (n=8). **b,** Changes in weight. **c–f,** Mice were sacrificed on day 7, and the colon (**c**) and spleen (**d**) were harvested. The colon length (**e**) and the spleen index (**f**) were quantified. **g, h,** The serum concentrations of IL-6 (**g**)

239 and TNF-α (**h**) were determined by ELISA when the mice were sacrificed on day 7. **i1-i6.**
240 Representative images of colons stained with hematoxylin and eosin and their quantitative
241 histological scores (**j**). Scale bar, 100 μm. **k1-k6,** Representative images of colons stained with
242 hematoxylin and MUC2 and their quantitative immunohistochemical scores (**l**). Scale bar, 100
243 μm. **m1-m6,** Representative images of colons stained with EdU (red) and WGA (green) and their
244 quantitative immunohistochemical scores (**n**). Scale bar, 100 μm. Representative images or
245 quantitative analyses of n=6 biologically independent samples are shown **(b-h, j l, n**). The data
246 are presented as the mean ± SD values. * $p < 0.05$, ** $p < 0.01$, *** $p < 0.001$, **** $p < 0.0001$
247 and ns (not significant) $p > 0.05$; the data were analyzed by ordinary one-way ANOVA (**b**) with
248 multiple comparison testing.
249 To further elucidate the mechanism underlying NALHP- and S6-mediated mucosal barrier
250 restoration, we employed multiomics approaches to analyze the whole-transcriptome and 16S
251 rRNA profiles of the colon and colon contents in DSS-treated mice. First, we investigated
252 whether the intestinal repair function of HP, as a carbohydrate, was attributable to short-chain
253 fatty acids generated through microbial metabolism in the gut. HP treatment did not alter the type
254 or composition of intestinal microbes in DSS-treated mice (Extended Data Fig. 10a-c). In
255 contrast, 5-ASA treatment led to the enrichment of genera such as *Porphyromonas*, *Neisseria*,
256 *Thermicanus*, and *Petrobacter* (Extended Data Fig. 10c), some of which have been associated
257 with exacerbated UC progression[31,32]. Notably, both NALHP and S6 improved the intestinal
258 microbial type and diversity in DSS-treated mice, increasing their similarity to the profiles

259 observed in wild-type (WT) mice (Extended Data Fig. 10a-c). Moreover, NALHP and S6
260 modulated the metabolite composition of the colonic contents, reducing the abundances of
261 inflammation-associated metabolites (Extended Data Fig. 10d). Integrated microbiome and
262 metabolome analyses revealed a significant positive correlation between gut microbial markers
263 in WT and DSS-treated mice (Extended Data Fig. 10e and f). The *genera Bacteroides* and
264 *Parabacteroides*, which were enriched in DSS-treated mice, were found to regulate the
265 metabolite profile. The abundances of *Prevotella* and *Sutterella* were significantly positively and
266 negatively correlated, respectively, with soluble colonic metabolites (Extended Data Fig. 10f).
267 NALHP and S6 treatment also affected the intestinal epithelial transcriptome in DSS mice,
268 altering the transcription of thousands of genes (Extended Data Fig. 11a). Enrichment analysis of
269 the genes associated with mucosal repair, including those involved in inflammation, metabolism,
270 and cell differentiation, revealed substantial changes in gene expression following treatment with
271 NALHP and S6 (Extended Data Fig. 11b). Further Gene Ontology (GO) analysis indicated that
272 mucosal barrier repair was a manifestation of the wound healing process, which was mediated
273 primarily through pathways such as the Notch and Wnt pathways, which regulate intestinal
274 epithelial cell development and regeneration in UC mice (Extended Data Fig. 11c). On the basis
275 of the results of the multiomics analysis, we concluded that the primary effects of NALHP and
276 S6 on DSS-induced colitis in mice were centered on the regulation of intestinal epithelial cell
277 development. During the active phase of UC, changes in epithelial cell proliferation occur at the
278 sites of colonic ulceration. Therefore, we selected PCNA as a marker of cell proliferation and

279 TCF1 as a downstream effector of the Wnt signaling pathway. Immunohistochemical staining
280 revealed that NALHP and S6 treatment normalized PCNA expression following ulceration and
281 restored TCF1 expression downstream of the Wnt pathway, but these effects were not observed
282 in mice treated with HP or 5-ASA (Extended Data Figs. 12 and 13).
283
284 ***NALHP & S6 promote goblet cell differentiation in UC organoids***
285 Intestinal organoids derived from human patients with inflammatory bowel disease (IBD) can
286 effectively recapitulate the absence of goblet cells clinically observed in vivo (Extended Data
287 Fig. 14 a and b). Therefore, we established a UC organoid model based on intestinal epithelial
288 cells isolated from the mucosal layer of Chinese patients diagnosed with ulcerative colitis
289 (Extended Data Fig. 15a). During the organoid culture process, NALHP, S6, and 5-ASA were
290 added to further investigate the potential mechanism by which deanticoagulated HP contributes
291 to the restoration of the mucosal barrier in UC mice, as observed above (Fig. 2). Morphological
292 analysis demonstrated that NALHP and S6 significantly altered the three-dimensional structural
293 features of the organoids during culture (Fig. 3a1-a3, Extended Data Video 1): compared with
294 those in the control group, the organoids in the NALHP/S6 groups exhibited decreased sphericity
295 (Fig. 3b) and an increased surface density and smoothness. In contrast, no morphological
296 alterations were observed following culture with 5-ASA (Fig. 3a4). To characterize the cellular
297 heterogeneity among the groups of organoids, single-cell transcriptome profiling was conducted.
298 The results revealed that the percentage of LGR5+ stem cells and PCNA+ transient amplifying

299 (TA) cells in the UC organoid control group was greater than 90% (Fig. 3c, d and Extended Data
300 Fig. 15b-e), confirming the robust proliferative and differentiation capabilities—which are
301 predominantly stem cell-driven—of these UC patient-derived organoids, as reported
302 previously[33]. Culture with NALHP or S6 induced substantial remodeling of the cellular
303 composition in the UC organoids: the percentage of stem/TA cells decreased to less than 10%,
304 whereas the percentage of goblet progenitor cells and their mature subtypes was greater than
305 80%. Additionally, approximately 5% of the intestinal epithelial cells exhibited markers of
306 differentiation, indicating that the culture of UC organoids with NALHP or S6 induced the
307 development of a functionally differentiated phenotype (Extended Data Fig. 15d and e), but no
308 functionally differentiated phenotype was detected in UC organoids cultured with 5-ASA (Fig.
309 3c and d).

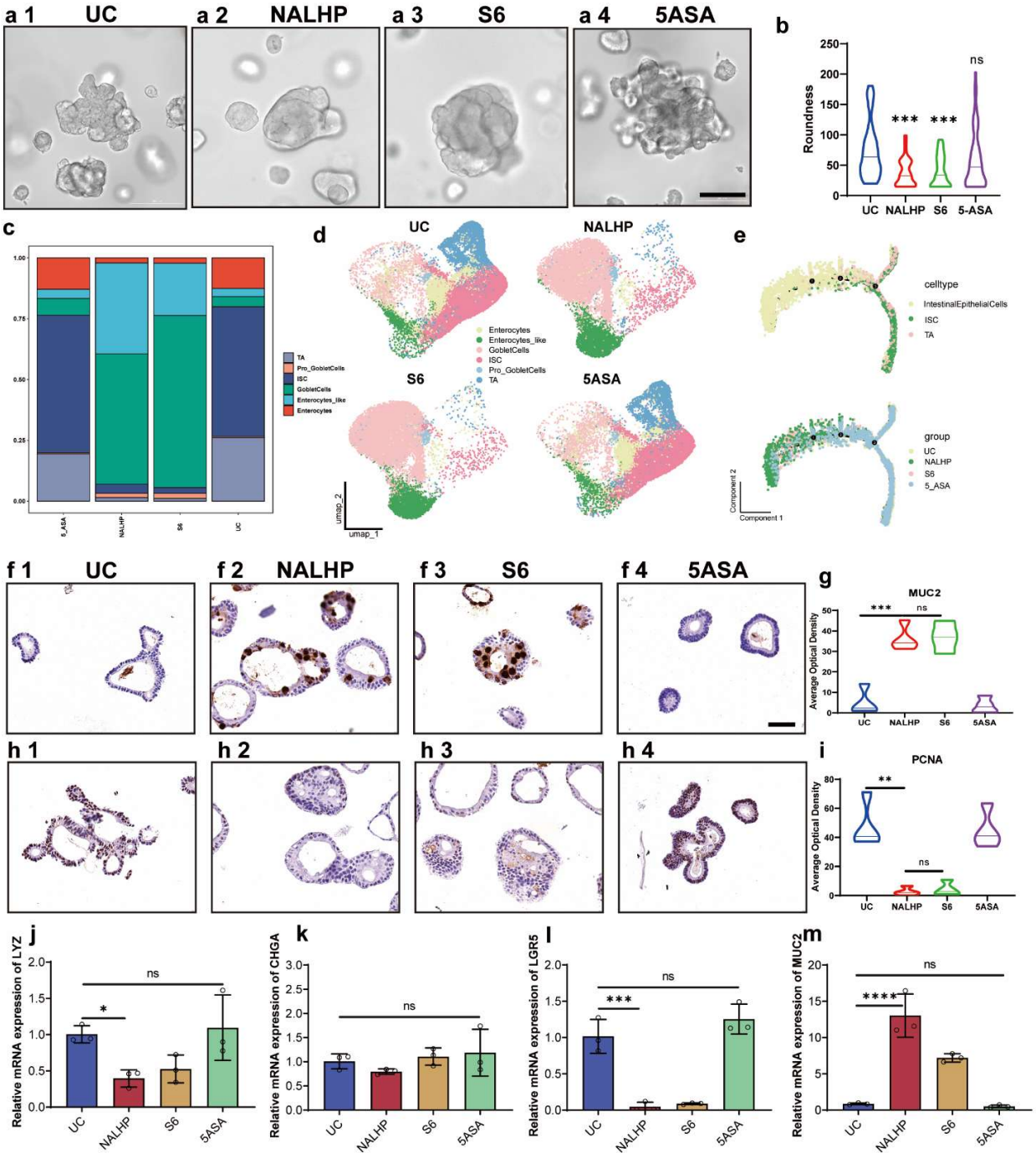

Fig. 3 NALHP and S6 promote the directed differentiation of goblet cells in organoids. a1–a4, Brightfield images of organoids. UC (a1), NALHP (a2), S6 (a3), and 5-ASA (a4) groups. **b,** Changes in the sphericity of the organoids. **c,** The percentages of cells in UC organoids in the

314 different groups. **d,** UMAP dimensionality reduction plot of UC organoids in the different

315 groups. **e,** Pseudotime analysis of UC organoids in the different groups and of cell types by

316 Monocle 2.**f1-f4.** Representative images of colons with hematoxylin and MUC2 staining and

317 quantitative immunohistochemical scores **(g)**. Scale bar, 50 μm. **h1-h4,** Representative images of

318 colons with hematoxylin and PCNA staining and quantitative immunohistochemical scores **(i)**.

319 Scale bar, 50 μm. **j–m,** Relative mRNA expression levels of LYZ **(j)**, CHGA **(k)**, LGR5 **(l)**, and

320 MUC2 **(m).**

321 Representative images or quantitative analysis results from n=3 biologically independent

322 samples are shown (**b, g, i, j-m**). The data are presented as the mean ± SD values. * $p < 0.05$, **

323 $p < 0.01$, *** $p < 0.001$, **** $p < 0.0001$ and ns (not significant) $p > 0.05$; the data were

324 analyzed by ordinary one-way ANOVA.

325 Furthermore, through the sequencing of temporal genes in the individual cells of UC organoids,

326 it was observed that organoids cultured with NALHP or S6 were composed of cells in the highly

327 differentiated stage, whereas the cells in the untreated group and in the group cultured with 5-

328 ASA remained in the early stage of differentiation (Extended Data Fig. 16a); moreover, the

329 highly differentiated cells originated from the intestinal stem cell–TA cell hierarchy in the

330 organoids (Fig. 3e), leading to a marked increase in the abundance of mucus-secreting goblet

331 cells (Extended Data Fig. 16b). Considering this differentiation pattern, we examined the

332 transcription of secretory cell markers and detected no significant differences in the mRNA

333 expression levels of lysozyme (LYZ) and chromogranin A (CHGA) among the groups (Fig. 3j

334 and k). However, the mRNA expression level of MUC2 significantly increased, whereas the
335 mRNA expression level of LGR5 significantly decreased when the organoids were cultured with
336 NALHP or S6 (Fig. 3l and m). On the basis of these findings, we hypothesized that the primary
337 function of NALHP and S6 is to mediate the directed differentiation of intestinal stem cells
338 toward the goblet cell lineage. Immunohistochemical analysis further confirmed that the
339 fluorescence intensity of the MUC2 protein was more than tenfold greater in the NALHP/S6-
340 treated groups than in the control UC and 5-ASA-treated groups (Fig. 3f1-f4), while the PCNA
341 signal was correspondingly reduced (Fig. 3h1-h4). These findings were highly consistent with
342 the results of the single-cell transcriptomic analysis (Fig. 3c). Moreover, the above results were
343 verified in organoids derived from three patients (Extended Data Figs. 15e and 17). Taken
344 together, these findings suggest that NALHP and S6 specifically promote the generation of
345 goblet cell lineages by activating the directed differentiation of intestinal stem cells in UC
346 organoids, thereby increasing the expression level of the mucin protein, similar to the effects
347 observed in mice with DSS-induced UC (Fig. 2k4, k5, and Extended Data Fig. 13).
348 Interestingly, during the process of dissociating organoids into single cells by treatment with
349 pancreatic enzymes, we found that the organoids in the NALHP/S6 culture groups were more
350 resistant to dissociation into single cells, suggesting stronger connections between the cells in the
351 UC organoids cultured with NALHP or S6 than between those in the control UC organoids.
352 Next, we stimulated NCM460 cells, a kind of normal human colonic epithelial cell, with IL-6 to
353 reduce the strength of the connections between cells mediated by the ZO-1 junction protein cells

354 and found that treatment with NALHP or S6 reversed the IL-6-induced damage to this tight
355 junction protein connecting NCM460 cells (Extended Data Fig. 18). These findings also suggest
356 that NALHP and S6 may restore the tight junction proteins connecting stimulated colonic
357 epithelial cells.
358
359 ***NALHP & S6 drive stem cell differentiation to goblet cells in UC organoids via separate***
360 ***Wnt/Notch inhibition***
361 UC organoids from the groups cultured with various drugs (NALHP, S6 and 5-ASA) and the
362 control group were collected and subjected to transcriptome analysis. KEGG and GO enrichment
363 analyses of the differentially expressed genes in the organoids cultured with NALHP and S6
364 revealed significant enrichment of these genes in the Wnt, Hippo, and Notch signaling pathways
365 (Extended Data Fig. 19a), which are key regulators of intestinal stem cell proliferation and
366 differentiation[33]. Notably, NALHP and S6 significantly inhibited the Wnt and Notch signaling
367 pathways through transcriptional regulation. Given that Wnt and Notch are critically involved in
368 the differentiation of intestinal stem cells[34], modulating their activity enables precise control over
369 the induction and differentiation of various intestinal epithelial cell types, including goblet cells.
370 Both NALHP and S6 promoted the differentiation of intestinal stem cells into goblet cells (Fig.
371 3j and m). Furthermore, when the UC organoids were cultured with the combination of the Wnt
372 pathway inhibitor IWP-2 and the Notch pathway inhibitor DAPT, the percentage of goblet cells
373 within the organoids increased to more than 60% (Extended Data Fig. 19b-e), which is consistent

374 with the mediation effects observed upon culture with NALHP or S6. To validate the central role
375 of Wnt and Notch pathway inhibition in NALHP/S6-mediated differentiation, functional rescue
376 experiments were conducted using CHIR99021 (C), a Wnt pathway agonist, and sodium
377 valproate (VPA, V), a Notch pathway agonist. In the presence of these agonists, the ability of
378 NALHP and S6 to promote the differentiation of intestinal stem cells (marked by LGR5) into
379 goblet cells (marked by MUC2) was partially abolished: UC organoid budding morphology was
380 restored (Extended Data Fig. 20), and the expression levels of Wnt- and Notch-related proteins,
381 whose expression was previously suppressed by NALHP/S6 treatment, were restored. Coculture
382 with the agonists significantly restored LGR5 expression and reduced MUC2 mRNA expression
383 ($p < 0.001$) in UC organoids (Fig. 4a and b). Additionally, the transcription and translation of
384 TCF1, a downstream effector of the Wnt pathway, were markedly inhibited in the agonist-treated
385 UC organoids (Fig. 4c and f). These findings clearly indicate that dual inhibition of the Wnt and
386 Notch pathways in UC organoids constitutes the primary mechanism underlying the biological
387 activity of NALHP/S6 in mediating the differentiation of goblet cells to increase the secretion of
388 mucosal layer components.

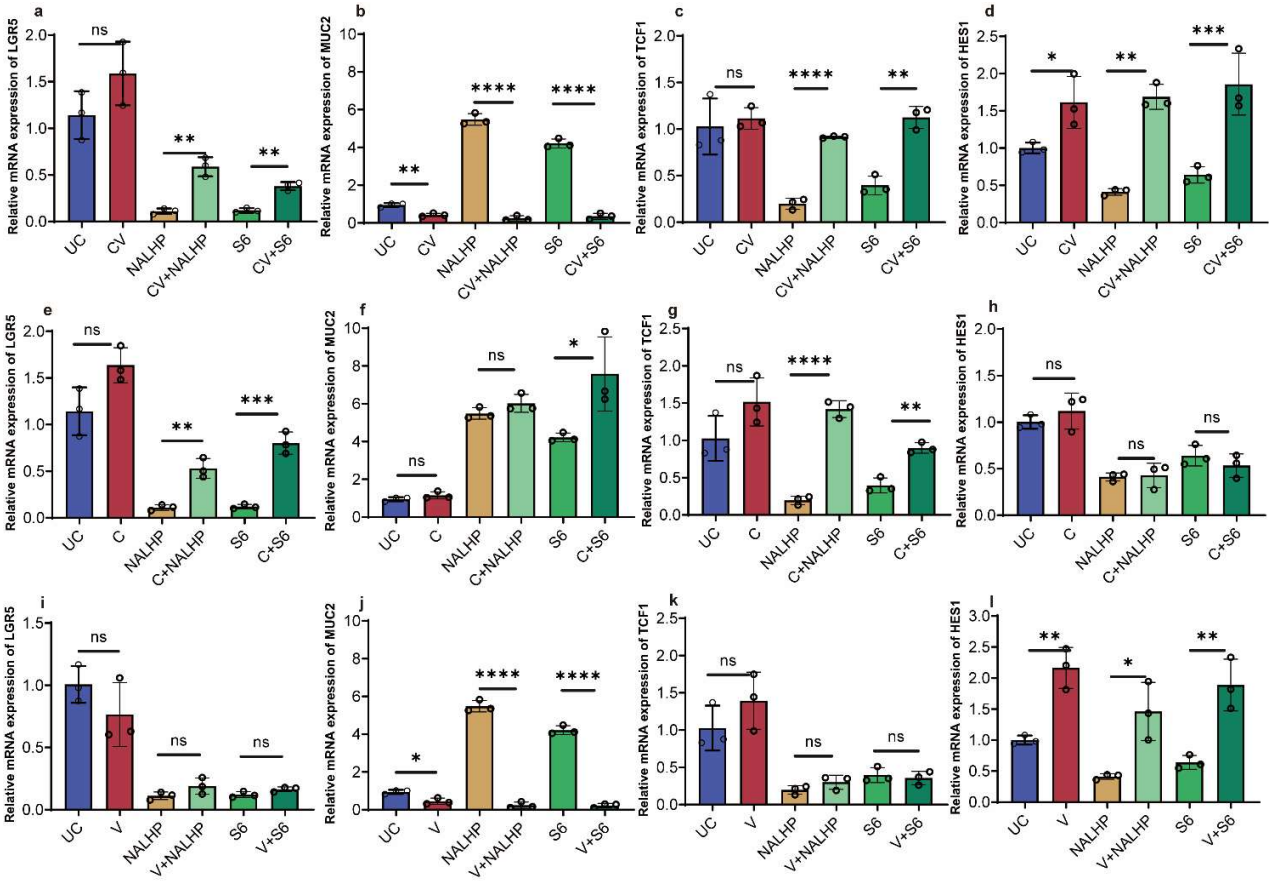

Fig. 4 Changes in UC organoids upon treatment with different inhibitors. a–d, The relative mRNA expression levels of LGR5 (**a**), MUC2 (**b**), TCF1 (**c**), and HES1 (**d**) in UC organoids after treatment with CHIR99021 (C), VPA (V) and NALHP/S6. **e-h,** The relative mRNA expression levels of LGR5 (**e**), MUC2 (**f**), TCF1 (**g**), and HES1 (**h**) in UC organoids after treatment with CHIR99021 (C) and NALHP or S6. **i–l,** The relative mRNA expression levels of LGR5 (**i**), MUC2 (**j**), TCF1 (**k**), and HES1 (**l**) in UC organoids after treatment with VPA (V) and NALHP or S6.

Representative results of the quantitative analysis of n=3 biologically independent samples are shown (**a–l**). The data are presented as the mean ± SD values. * $p < 0.05$, ** $p < 0.01$, *** $p <$

399 0.001, **** $p < 0.0001$ and ns (not significant) $p > 0.05$; the data were analyzed by ordinary one-
400 way ANOVA.
401 During the development of the intestinal tract, Wnt and Notch signaling can determine the fate of
402 intestinal stem cells. We selected the downstream effectors TCF1 and HES1, which are related to
403 the Wnt and Notch signaling pathways, to further determine the influence of these pathways. The
404 expression level of HES1 during the development of goblet cells is highly important. High
405 expression levels of HES1 inhibit the process of differentiation toward goblet cells. Culture with
406 NALHP or S6 led to significant inhibition of Hes1 and TCF1 mRNA expression (Fig. 4c and d),
407 and agonist treatment partially reversed this effect, with a consistent effect at the translational
408 level (Extended Data Fig. 21). To determine the individual contributions of each pathway,
409 CHIR99021 and VPA were applied separately in combination with NALHP or S6. Gene
410 expression analysis revealed that CHIR99021 restored LGR5 mRNA expression (indicative of
411 stemness) (Fig. 4e) and activated the Wnt signaling pathway (Fig. 4g and Extended Data Fig. 22)
412 but did not inhibit the upregulation of MUC2 (Fig. 4f) or regulate the Notch signaling pathway
413 (Fig. 4h). Conversely, VPA suppressed the induction of MUC2 expression by activating the
414 Notch signaling pathway (Fig. 4j, m and Extended Data Fig. 23), but it did not regulate the Wnt
415 signaling pathway (Fig. 4k) to restore the expression of LGR5 (Fig. 4i). Collectively, these
416 results demonstrate that NALHP and S6 exert their effects by coordinately modulating both the
417 Wnt and Notch pathways to drive the directed differentiation of intestinal stem cells into goblet
418 cells.

419 **Discussion**

420 The absence of a mucus layer and the impairment of the intestinal epithelial barrier—
421 pathological features whose complexity imposes stringent demands on existing therapeutic
422 agents—are the central challenges in UC treatment[35]. In the development of anti-UC
423 medications, HP, a classic anticoagulant drug, has demonstrated potential in alleviating intestinal
424 inflammation. However, the data from nearly three decades of trial-and-error studies reveal
425 substantial variability and even contradictory outcomes regarding its efficacy; these limitations
426 are compounded by the inherent hemorrhagic risks of these drugs, preventing the in-depth and
427 broad exploration of their nonanticoagulant activity. In this study, we innovatively propose the
428 critical hypothesis that the anticoagulant activity of HP enriched during drug production may
429 interfere with its anti-UC effects. By employing the strong oxidation performance of sodium
430 periodate to open the ring of glucuronic acid, one of the anticoagulant pentasaccharides[3], the
431 ability of sodium borohydride reduction to stabilize the open ring structure, and subsequent
432 depolymerization by heparinase I[3], we obtained a novel deanticoagulated HP derivative, NALHP,
433 which has no anticoagulant activity but does exhibit stable and effective anti-UC activity (Fig.
434 1a, Extended Data Figs. 2 and 3).

435 The interference of anticoagulant activity enriched during heparin drug manufacturing is one of
436 the reasons that the nonanticoagulant activity of conventional heparin drugs is difficult to
437 explore. We have adopted various methods to prepare heparin derivatives without anticoagulant
438 activity. The derivative III,II-2-Odes, which does not contain sulfonate groups, did not exhibit

439 significant therapeutic activity against UC. The derivative NAHP, obtained by opening the ring
440 with potassium periodate, exhibited obvious therapeutic activity against UC, indicating that
441 sulfonation is one of the key factors for the ability of heparin to treat UC. Molecular weight is
442 another key factor for the release of heparin activity. Chemical degradation of Eno and NAEno
443 did not result in a therapeutic effect on UC, indicating that chemical degradation destroys the
444 active anti-UC fragments. Therefore, we used our previously established heparinase expression
445 system and expressed heparinases I, II, and III. Using the recombinant heparinases, we
446 controlled the reduction in the molecular weight of NAHP to obtain NALHP, NAULHP and 11
447 fine separation fragments from the NALHP (Extended Data Fig. 3, Extended Data Table.1).
448 The reduction in molecular weight increased the therapeutic activity against UC, but NALHP
449 treatment resulted in a higher survival rate in UC model mice. In addition, among the 11
450 separated fragments, the efficacy of S6 is consistent with that of NALHP, the efficacy of S4 is
451 like that of NAULHP, and S10 shows no significant efficacy, indicating that an appropriate
452 molecular weight (3000Da-8000Da) is another key factor for the ability of deanticoagulated
453 heparin to treat UC (Extended Data Fig. 4j, Extended Data Table.1). The unique structural
454 modification of the anticoagulant pentasaccharide domain[3] in NALHP not only eliminated the
455 anticoagulant properties of HP but also resulted in anti-UC activity. The formation of gsGlcA
456 results from redox reaction-induced ring opening of glucuronic acid residues, whereas Δ4,5-
457 unsaturated glucuronic acid is a characteristic product generated during the heparinase I-
458 mediated cleavage of glycosidic bonds (Fig. 1e-g and Extended Data Fig. 9).

459 The primary structural differences between HP and NALHP are the presence and absence,
460 respectively, of the active anticoagulant pentasaccharide sequence and variations in the
461 molecular weight distribution. Thus, this unique preparation process enabled the discovery of the
462 unique therapeutic mechanism of deanticoagulated HP derivatives in UC. NALHP has a broad
463 molecular weight distribution (PDI=2.23). After separation by gel chromatography, fragment S6,
464 with a molecular weight within the range of 3000Da to 5000Da and a PDI of 1.1 and accounting
465 for 15.3% of the structure of NALHP (Extended Data Table 1 and Extended Data Fig. 3), had the
466 same or an even greater therapeutic effect on UC relative to NALHP (Fig. 2). We also attempted
467 to change the order of preparation of the nonanticoagulant by sodium borohydride reduction and
468 enzymatic depolymerization of HP and found that NAI45, a product generated by an initial
469 enzymatic reaction resulting in a low molecular weight followed by a reaction resulting in the
470 nonanticoagulant property[3], did not exhibit therapeutic activity against UC (Extended Data Fig.
471 4), indicating that the unique preparation route is also one of the reasons that the different
472 structure of NALHP allows it to exert therapeutic effects on UC (Extended Data Figs. 2 and 4).
473 In addition, we cultured organoids with fondaparinux sodium and nonanticoagulant fondaparinux
474 sodium but found that it did not have the same effect as NALHP did (Extended Data Fig. 24).
475 These results indicate that the intestinal stem cell differentiation-promoting activity and
476 anticoagulant activity are independent in HP molecules. We also further explored the effects of
477 the S6 administration method. Intravenous injection, intraperitoneal injection, and subcutaneous
478 injection failed to achieve the effects of oral S6 in repairing the intestinal mucosal barrier of mice

479 with DSS-induced colon damage (Extended Data Fig. 5). Oral administration is the best route for
480 NALHP/S6 to exert their effects.
481 To elucidate how NALHP/S6 alleviate UC, comprehensive in vitro and in vivo experiments
482 using DSS-treated mice were conducted. Initial observations indicated that oral NALHP
483 administration reduced inflammatory cell infiltration in colonic crypts, decreased serum
484 inflammatory cytokine concentrations, and restored the orderly proliferation of damaged crypt
485 structures in DSS-treated mice, effects that collectively ameliorated UC pathology (Fig. 2).
486 Subsequent multiomics analysis revealed that the mechanism underlying the effects of NALHP
487 in UC model mice is dependent on intestinal epithelial wound healing and stem cell
488 proliferation/differentiation (Extended Data Figs. 10 and 11). Further validation using a human
489 patient-derived UC organoid model revealed that NALHP/S6 restored the differentiation
490 trajectory of LGR5+ stem cells, in turn increasing the proportion of mucus-secreting goblet cells
491 in UC organoids from <10% to ≥80% (Fig. 3c), which was consistent with the findings in the
492 mouse model (Extended Data Figs. 11-13). This unique differentiation-promoting mechanism
493 effectively repaired colonic crypt structural units, reestablishing the dual protection offered by
494 the intestinal mechanical and chemical barriers. Transcriptome analysis revealed significant
495 alterations in UC organoids after NALHP treatment (Extended Data Fig. 19), particularly
496 inhibition of the Wnt and Notch pathways, which are associated with crypt stem cell
497 proliferation/differentiation. The results of mechanistic rescue experiments confirmed that
498 NALHP primarily suppressed these pathways to drive stem cell differentiation (Fig. 4, Extended

499 Data Fig. 20 and Extended Data Videos 1-6). These findings indicate that NALHP/S6 not only
500 alleviates UC by inhibiting inflammatory responses, as do 5-ASA[36] and infliximab, but also
501 promotes the repair of the mucosal layer barrier at a deeper level to cure UC.
502 As all intestinal crypt cells originate from LGR5+ stem cells at the crypt base, crypt destruction
503 contributes to the refractory nature of UC[37-39]. Endoscopic mucosal healing is considered the
504 gold standard for the success of clinical UC therapy. Using UC mouse model and human patient-
505 derived UC organoid model, we proved that NALHP/S6 promoted goblet cell differentiation in
506 the mucus layer, reduced the abnormal proliferation of intestinal stem cells and reinforced the
507 crypt self-renewal capacity by regulating the Wnt and Notch signaling pathways (Fig. 4 and
508 Extended Data Fig. 19), thereby repairing the intestinal mucosal barrier and disrupting the
509 malignant pathological cycle of UC. This study demonstrates for the first time that the
510 deanticoagulated HP derivatives NALHP and S6 exert mucosal barrier repair effects by
511 regulating crypt stem cell fate, offering an innovative strategy to overcome the limitations of
512 current drugs in UC therapy. The successful development of NALHP provides a promising
513 strategy for identifying the pleiotropic mechanisms of glycosaminoglycan-based drugs, which
514 has substantial translational value.
515

References

1. Villablanca, E. J., Selin, K. & Hedin, C. R. H. Mechanisms of mucosal healing: treating inflammatory bowel disease without immunosuppression? *Nat. Rev. Gastroenterol. Hepatol.* **19**, 493–507 (2022).
2. Alsoud, D., Verstockt, B., Fiocchi, C. & Vermeire, S. Breaking the therapeutic ceiling in drug development in ulcerative colitis. *Lancet Gastroenterol. Hepatol.* **6**, 589–595 (2021).
3. Ji, Y. et al. A heparin derivatives library constructed by chemical modification and enzymatic depolymerization for exploitation of non-anticoagulant functions. *Carbohydr. Polym.* **249**, 116284 (2020).
4. Feuerstein, J. D. et al. AGA clinical practice guidelines on the management of moderate to severe ulcerative colitis. *Gastroenterology* **158**, 1450–1463 (2020).
5. Ulcerative colitis. *Journal* **6**, 73 (2020). doi: 10.1038/s41572-020-00215-4
6. Alatab, S. et al. The global, regional, and national burden of inflammatory bowel disease in 195 countries and territories, 1990-2017: a systematic analysis for the Global Burden of Disease Study 2017. *Lancet Gastroenterol. Hepatol.* **5**, 17–30 (2020).
7. Gajendran, M. et al. A comprehensive review and update on ulcerative colitis. *Dis. Mon.* **65**, 100851 (2019).
8. Abraham, C. & Cho, J. H. Inflammatory bowel disease. *N. Engl. J. Med.* **361**, 2066–2078 (2009).

9. Beaugerie, L. & Itzkowitz, S. H. Cancers complicating inflammatory bowel disease reply. *N. Engl. J. Med.* **373**, 195–195 (2015).

10. Nakase, H. et al. Evidence-based clinical practice guidelines for inflammatory bowel disease 2020. *J. Gastroenterol.* **56**, 489–526 (2021).

11. Singh, S., Murad, M. H., Fumery, M., Dulai, P. S. & Sandborn, W. J. First- and second-line pharmacotherapies for patients with moderate to severely active ulcerative colitis: an updated network meta-analysis. *Clin. Gastroenterol. Hepatol.* **18**, 2179–2191.e6 (2020).

12. Mowat, C. et al. Guidelines for the management of inflammatory bowel disease in adults. *Gut* **60**, 571–607 (2011).

13. Peyrin-Biroulet, L. & Lémann, M. Review article: remission rates achievable by current therapies for inflammatory bowel disease. *Aliment. Pharmacol. Ther.* **33**, 870–879 (2011).

14. Okayasu, M., Ogata, H. & Yoshiyama, Y. Use of corticosteroids for remission induction therapy in patients with new-onset ulcerative colitis in real-world settings. *J. Mark. Access Health Policy* **7**, 1565889 (2019).

15. Kayal, M. & Shah, S. Ulcerative colitis: current and emerging treatment strategies. *J. Clin. Med.* **9**, 12 (2020).

16. Bhattacharya, A. & Osterman, M. T. Biologic therapy for ulcerative colitis. *Gastroenterol. Clin. N. Am.* **49**, 717–729 (2020).

17. Hirten, R. P. & Sands, B. E. New therapeutics for ulcerative colitis in *Annual Review of*

556 *Medicine* (ed M. E. Klotman) 199–213 (Annual Reviews, 2021).

557 18. Mulloy, B., Hogwood, J., Gray, E., Lever, R. & Page, C. P. Pharmacology of heparin and
558 related drugs. *Pharmacol. Rev.* **68**, 76–141 (2016).

559 19. Oduah, E. I., Linhardt, R. J. & Sharfstein, S. T. Heparin: past, present, and future.
560 *Pharmaceuticals (Basel, Switzerland)* **9**, 38 (2016).

561 20. Cui, J. et al. Highly sensitive and selective detection of heparin in serum based on a long-
562 wavelength tetraphenylethylene-cyanopyridine aggregation-induced emission luminogen.
563 *Anal. Chem.* **92**, 7106–7113 (2020).

564 21. Gray, E., Hogwood, J. & Mulloy, B. The anticoagulant and antithrombotic mechanisms of
565 heparin in *Heparin - A Century of Progress. Handbook of Experimental Pharmacology*
566 (eds R. Lever, B. Mulloy, & C. Page) 43–61 (Springer, 2012).

567 22. Ang, Y. S. et al. Randomized comparison of unfractionated heparin with corticosteroids
568 in severe active inflammatory bowel disease. *Aliment. Pharmacol. Ther.* **14**, 1015–1022
569 (2000).

570 23. Ludwig, R. J. et al. The ability of different forms of heparins to suppress P-selectin
571 function in vitro correlates to their inhibitory capacity on bloodborne metastasis in vivo.
572 *Thromb. Haemost.* **95**, 535–540 (2006).

573 24. Kim, S. Y. et al. Glycosaminoglycan compositional analysis of relevant tissues in Zika
574 virus pathogenesis and in vitro evaluation of Heparin as an antiviral against Zika virus
575 infection. *Biochemistry* **58**, 1155–1166 (2019).

576 25. Gaffney, P. R. et al. Paradoxical response to heparin in 10 patients with ulcerative-colitis.
577 *Am. J. Gastroenterol.* **90**, 220–223 (1995).
578 26. Törkvist, L. et al. Low molecular weight heparin as adjuvant therapy in active ulcerative
579 colitis. *Aliment. Pharmacol. Ther.* **13**, 1323–1328 (1999).
580 27. Zezos, P. et al. Low-molecular-weight heparin (enoxaparin) as adjuvant therapy in the
581 treatment of active ulcerative colitis: a randomized, controlled, comparative study.
582 *Aliment. Pharmacol. Ther.* **23**, 1443–1453 (2006).
583 28. Chande, N., MacDonald, J. K., Wang, J. J. & McDonald, J. W. D. Unfractionated or low
584 molecular weight heparin for induction of remission in ulcerative colitis: a cochrane
585 inflammatory bowel disease and functional bowel disorders systematic review of
586 randomized trials. *Inflamm. Bowel Dis.* **17**, 1979–1986 (2011).
587 29. Huang, L. et al. "Two-birds-one-stone" oral nanotherapeutic designed to target intestinal
588 integrins and regulate redox homeostasis for UC treatment. *Sci. Adv.* **10**, eado7438
589 (2024).
590 30. Darwish, N. H. E., Godugu, K. & Mousa, S. A. Sulfated non-anticoagulant low molecular
591 weight heparin in the prevention of cancer and non-cancer associated thrombosis without
592 compromising hemostasis. *Thromb. Res.* **200**, 109–114 (2021).
593 31. Hirano, A. et al. Comparison of the microbial community structure between inflamed and
594 non-inflamed sites in patients with ulcerative colitis. *J. Gastroenterol. Hepatol.* (2018).
595 32. Zhao, X. et al. Porphyromonas gingivalis exacerbates ulcerative colitis via

596 Porphyromonas gingivalis peptidylarginine deiminase. *Int. J. Oral Sci.* **13**, 31 (2021).

597 33. Malagola, E. et al. Isthmus progenitor cells contribute to homeostatic cellular turnover
598 and support regeneration following intestinal injury. *Cell* **187**, 3056–3071.e17 (2024).

599 34. Yin, X. et al. Niche-independent high-purity cultures of Lgr5+ intestinal stem cells and
600 their progeny. *Nat. Methods* **11**, 106–112 (2014).

601 35. Hirten, R. P. & Sands, B. E. New therapeutics for ulcerative colitis. *Annu. Rev. Med.* **72**,
602 199–213 (2021).

603 36. Tang, S. et al. Sustained release of 5-aminosalicylic acid from azoreductase-responsive
604 polymeric prodrugs for prolonged colon-targeted colitis therapy. *J. Nanobiotechnology*
605 **22**, 468 (2024).

606 37. Schlegel, N. Promoting mucosal healing by targeting TMEM219-dependent intestinal
607 epithelial stem cell defects in inflammatory bowel disease. *J. Clin. Invest.* **135**, e192640
608 (2025).

609 38. Sarvestani, S. K. et al. Induced organoids derived from patients with ulcerative colitis
610 recapitulate colitic reactivity. *Nat. Commun.* **12**, 262 (2021).

611 39. Wu, J. et al. EFHD2 suppresses intestinal inflammation by blocking intestinal epithelial
612 cell TNFR1 internalization and cell death. *Nat. Commun.* **15**, 1282 (2024).

613 **Methods**

614

615 ***Preparation of deanticoagulated HP derivatives***[3]

616 The preparation process of deanticoagulated HP derivatives was described previously. Briefly,
617 pharmaceutical-grade HP sodium was purchased from Changshan Biochemical Pharmaceutical
618 Co., Ltd. (Hebei, China). To eliminate anticoagulant activity, HP was dissolved in water at a
619 concentration of 33 mg/ml. The solution was reacted with an equal volume of 0.2 M periodate
620 sodium solution at 4 °C for 22 hr prior to neutralization reactions with 4 ml of glycol and 1.4 g of
621 sodium borohydride per gram of HP at 4 °C for 1 hr and 16 hr, respectively. The resulting
622 solution was adjusted to pH 7.0, filtered through a membrane, desalted using a 3 kDa Pellicon 2
623 Mini Cassette (Millipore, Germany), and lyophilized to obtain deanticoagulated HP (NAHP).
624 NAHP was subsequently subjected to further enzymolysis with heparinase I (Beijing Bio-Cell
625 Technology Co., Ltd., China). NAHP was dissolved in a reaction buffer consisting of 20 mM
626 Tris, 200 mM NaCl, and 5 mM $CaCl_2$ at pH 7.4. The increase in the absorbance at 232 nm was
627 recorded immediately after heparinase I was added to the NAHP solution. Low-molecular-weight
628 NAHP (NALHP) and ultra-low-molecular-weight NAHP (NAULHP) were obtained when the
629 absorbance increased to 45 and 100, respectively. The excess heparinase I was inactivated once
630 the increase reached the endpoint by heating the solution at 100 °C for 10 min. The solution was
631 filtered, precipitated with alcohol, and lyophilized to obtain NALHP and NAULHP. The HP
632 derivative NAI45 was prepared through the enzymolysis of HP using heparinase I, allowing the

633 increase in the absorbance to reach 45, followed by periodate sodium oxidation and sodium
634 borohydride reduction. The nonanticoagulant enoxaparin (NAEno) was prepared from
635 commercial enoxaparin (Changshan Biochemical Pharmaceutical Co., Ltd., Hebei, China) using
636 the same preparation process used for the oxidation of HP to NAHP.
637
638 ***Molecular Weight Determination of deanticoagulated HP Derivatives***
639 The molecular weight of each HP derivative was determined using gel penetration
640 chromatography (GPC) as described previously. In short, an HPLC system (Waters, America)
641 with a binary pump module, an autosampler, and a refractive index detector was used. The
642 mobile phase consisted of 0.2 M sodium sulfate solution at pH 5.0. HP derivatives, the HP
643 sodium molecular weight calibrant (USP, America), and low-molecular-weight HP for molecular
644 weight calibration (NIBSC, America) were dissolved in the mobile phase at a concentration of 20
645 mg/ml. The samples were subsequently injected onto a 300 × 7.8-mm TSK Gel G2000SW$_{XL}$
646 column (Tosoh, Japan) in a volume of 25 μl. The column was eluted at a flow rate of 0.5 ml/min
647 and a temperature of 35 °C. The data were collected and analyzed in Breeze 2 (Waters, America)
648 software. The molecular weight distributions of the HP derivatives were calculated based on the
649 standard curve generated from the calibrant with a general third-order calibration method.
650
651 ***Fine separation of the NALHP***
652 Fine separation of the HP derivatives was performed using a HiPrep 16/60 Sephacryl S-100 HR

653 column (GE Healthcare, America) with a ÄKTA prime purification system (GE Healthcare,
654 America). The mobile phase consisted of 0.2 M sodium chloride solution at pH 5.0. The HP
655 derivative NALHP was dissolved in the mobile phase at a concentration of 120 mg/ml. The
656 sample was subsequently injected onto the column using a 5 ml injection loop. The column was
657 eluted at a flow rate of 0.5 ml/min at room temperature. Fractions were collected every 10 min
658 from 70 min to 180 min after sample injection and were designated S1 to S11 according to the
659 order of retention time. Afterward, the samples were lyophilized and reconstituted in water at
660 30% of the original volume to enrich polysaccharides, and alcohol precipitation and another
661 lyophilization step were then performed to obtain the separated components.
662
663 ***Mouse model of DSS-induced colitis***
664 Male C57BL/6J mice (18–22 g, 6–8 weeks) were purchased from Vital River Laboratories
665 (Beijing, China). The mice were housed under specific pathogen-free conditions in the laboratory
666 animal facility of Tsinghua University. The animal protocols 17-XXH1 and 20-XXH1 were
667 carried out with the approval of the Institutional Animal Care and Use Committee (IACUC) of
668 Tsinghua University. The laboratory animal facility was accredited by AAALAC (Association
669 for Assessment and Accreditation of Laboratory Animal Care) International.
670 Evaluation of the anti-UC efficacy of the HP derivatives was performed using a 7-day mouse
671 model of acute colitis. All the mice were pre-fed for one week prior to any subsequent
672 experiments. The mice were given 3% DSS (dextran sulfate sodium; colitis grade, MP

673 Biomedicals, America) solution instead of water for 7 consecutive days. The HP derivatives and
674 5-aminosalicylic acid (5-ASA) were dissolved in saline at a concentration of 3 mg/ml. Starting 3
675 days post-DSS induction, the mice were orally administered the drug solution daily at a dosage
676 of 30 mg/kg/d. The mice were euthanized by CO_2 inhalation after DSS induction for 7 days. The
677 serum was separated from the cardiac blood of the mice, while the spleens and the colons were
678 excised and measured. The colon tissue was cut in the longitudinal direction, washed with ice-
679 cold PBS, rolled with the Swiss-rolling technique, fixed, and embedded in paraffin for further
680 investigations.
681 Multiomics analyses were performed in a 14-day mouse colitis model to evaluate the systemic
682 changes in mice with colitis caused by drugs. The mice were allowed to drink 3% DSS solution
683 for 3 days, after which they received standard drinking water and drug treatment for 4 days.
684 Afterward, the mice were allowed to drink 2% DSS solution for another 3 days, after which they
685 received standard drinking water and drug treatment for another 4 days. Fresh feces were
686 collected prior to euthanasia by CO_2 inhalation. After the mice were sacrificed, the colons were
687 removed. The colonic contents were collected while the colonic epithelial tissue was scraped and
688 collected in 1.5 ml centrifuge tubes containing TRIzol reagent (Invitrogen, America).
689
690 ***ELISA***
691 The concentrations of interleukin-6 (IL-6) and tumor necrosis factor-alpha (TNF-α) in serum and
692 cell culture medium were measured using an IL-6 Mouse ELISA Kit (Invitrogen, America) and a

693 TNF-α Mouse ELISA Kit (Invitrogen, America), respectively, according to the manufacturer's

694 instructions.

695

696 ***Principal Component Analysis (PCA)***

697 The data matrix was standardized to unit variance to prevent scale bias. A covariance matrix was

698 computed and decomposed into eigenvalues and eigenvectors. Principal components

699 explaining >70–80% cumulative variance, or meeting Kaiser's criterion (eigenvalue >1), were

700 retained. Component scores were calculated by projecting data onto eigenvectors, and loadings

701 were computed to interpret trait contributions. A biplot visualized sample clustering and trait

702 relationships in the first two or three PCs. Analyses used the vegan (v.2.5–7) and ggplot2

703 (v.3.3.5) packages, with standard PCA functions post-preprocessing.

704

705 ***Biolayer interferometry***

706 The molecular interactions between DSS and the HP derivatives were evaluated using an Octet

707 Red96 instrument (FortéBIO, America). DSS and the HP derivatives were dissolved in HBS-EP

708 buffer containing 10 mM HEPES, 150 mM NaCl, 3 mM EDTA, and 0.005% Tween 20 at pH

709 7.4. The streptavidin sensors were loaded with DSS washed in HEB-EP buffer and exposed to

710 the HP derivatives.

711

712 ***RNA isolation and qPCR***

713 Total RNA was extracted using TRIzol reagent (Invitrogen) and reverse transcribed to cDNA
714 using a FastKing RT Kit (TIANGEN, China). All qPCRs were run in a CFX96 Touch Real-Time
715 PCR Detection System (Bio-Rad, America) using Talent qPCR PreMix (TIANGEN, China) with
716 the specific primers listed in the extended data.
717
718 ***FTIR spectroscopy***
719 The infrared absorption spectra of the HP derivatives were generated using a Nicolet 6700 FTIR
720 spectrometer (Thermo Electron Corporation, Shanghai, China) with the potassium bromide tablet
721 method. The spectral data were collected in a 4000–400 cm^{-1} range for all the samples.
722
723 ***NMR analysis***
724 For 1D (^{1}H, ^{13}C) and 2D-NMR analyses, HP derivatives (50–60 mg) were dissolved in 0.6 mL of
725 deuterium oxide and lyophilized repeatedly to remove exchangeable protons. The thoroughly
726 dried samples were then dissolved in 0.5 mL of deuterium oxide with 0.002% 3-(trimethylsilyl)
727 propionate sodium salt (TSP) and transferred into 25 × 0.5-cm NMR tubes (Wilmad Lab Glass,
728 America). 1D (^{1}H, ^{13}C) and 2D-NMR experiments were performed at 298 K on a Bruker
729 Advance 600 MHz spectrometer (Germany) equipped with a 5 mm helium-cooled cryoprobe
730 using the following parameters: Proton—number of scans, 16; number of dummy scans, 2;
731 relaxation delay, 1.0 s; spectral width, 20 ppm; and transmitter offset, 6.0 ppm. One-dimensional
732 ^{13}C spectra were obtained with proton decoupling during acquisition at 298 K over 5000 scans.

733 All the spectra were Fourier transformed, phased and baseline corrected. The chemical shift
734 values were calibrated with TSP at 0.00 ppm. HSQC spectra were recorded with carbon
735 decoupling during acquisition with 256 increments of 16 scans. The polarization transfer delay
736 was set for a $^{1}J_{C\text{-}H}$ coupling value of 145 Hz.
737
738 ***Microbiome analysis***
739
740 *Sample preparation and DNA extraction*
741 Fresh fecal samples from colitis model mice were collected in 1.5-ml centrifuge tubes and stored
742 immediately at –80 °C until further analysis. Microbial genomic DNA samples were extracted
743 using a DNeasy PowerSoil Kit (QIAGEN, Germany) following the manufacturer's instructions.
744 The DNA concentrations in the samples were subsequently quantified using a NanoDrop ND-
745 1000 spectrophotometer (Thermo Fisher Scientific, America), and the samples were then
746 qualified by agarose gel electrophoresis.
747
748 *16S rRNA amplicon sequencing*
749 The V3–V4 region of the bacterial 16S rRNA gene was amplified by PCR using the forward
750 primer 338F (5'-ACTCCTACGGGAGGCAGCA-3') and the reverse primer 806R (5'-
751 CGGACTACHVGGGTWTCTAAT-3'). Sample-specific 7-bp barcodes were added to the
752 primers for further multiplex sequencing. PCR amplicons were purified using VAHTS™ DNA

753 Clean Beads (Vazyme, China) and quantified using a PicoGreen dsDNA Assay Kit (Invitrogen,
754 America) prior to manipulation to achieve equal amounts of DNA. Afterward, paired-end 2 ×
755 250 bp sequencing was performed on the MiSeq platform (Illumina, America) with a NovaSeq
756 6000 SP Reagent Kit.
757
758 *Microbiome data analysis*
759 The raw sequence data were processed with QIIME2 2019.4 (Bolyen *et al*. 2018) with slight
760 modifications based on the official tutorials (https://docs.qiime2.org/2019.4/tutorials/). In brief,
761 the raw data were demultiplexed with the demux plugin, and primers were removed with the cut
762 adapt plugin. Afterward, the data were subjected to quality filtering, denoising, merging, and
763 chimera removal with the DADA2 plugin. A count table without rarefaction was used for further
764 analysis. The following analysis was carried out using an in-house-developed R script in Rstudio
765 software (v.2021.09.1, R version 4.1.2). Alpha diversity analysis and principal coordinate
766 analysis (PcoA) were performed using the vegan (v.2.5-7) package. Enterotyping was performed
767 with the Dirichlet multinomial mixture model with the DirichletMultinomial (v.1.36.0) package.
768 Data visualization was performed using the ggplot2 (v.3.3.5) and ggalluvial (v.0.12.3) packages.
769 In addition, LefSe analysis was performed on the Genescloud platform
770 (https://www.genescloud.cn/home).
771
772 ***Metabolome analysis***

773

774 *Sample preparation and extraction*

775 Samples of the colonic contents were thawed on ice. Aqueous homogenates were obtained by
776 mixing 100 mg of each sample with 300 μl of ice-cold water and steel balls for 5 min prior to
777 incubation on ice for 10 min. Then, 500 μl of methanol was added, and the homogenates were
778 mixed by vortexing for 5 min prior to incubation on ice for another 10 min. The homogenates
779 were centrifuged (12,000 rpm, 4 °C, 10 min), and 600 μl of the supernatant was transferred to
780 1.5-ml centrifuge tubes for further concentration. The concentrated dry products were dissolved
781 in 100 μl of 5% methanol–water, vortexed, and centrifuged (12,000 rpm, 4 °C, 10 min). Finally,
782 the supernatants were collected for LC–MS/MS analysis.

783

784 *LC–MS analysis*

785 A combination of positive ion mode MS and negative ion mode MS was applied to identify the
786 metabolites in the colonic contents. Data were acquired with an LC–MS system comprising a
787 1290 Infinity LC System (Agilent, America) coupled to a 6545 LC/Q-TOF mass spectrometer
788 (Agilent, America). The method details are summarized as follows. The supernatants were
789 injected onto a 100 × 2.1-mm ACQUITY UPLC HSS T3 C18 column (Waters, America) in a
790 volume of 2 μl. The column was eluted at a flow rate of 400 μl/min and a temperature of 40 °C.
791 Mobile phase A (water with 0.1% formic acid) and mobile phase B (acetonitrile with 0.1%
792 formic acid) were used with the following gradient program: 95:5 V/V A:B at 0 min, 10:90 V/V

793 at 11.0 min, 10:90 V/V at 12.0 min, 95:5 V/V at 12.1 min, 95:5 V/V at 14.0 min. In positive ion
794 mode, MS analysis was carried out using the following settings: ion spray voltage, 250; gas flow,
795 8; fragmentor, 135; gas temperature, 325 °C; sheath temperature, 325 °C; sheath flow, 11; and
796 nebulizer, 40. In negative ion mode, MS analysis was carried out using the following settings:
797 ion spray voltage, 1,500; gas flow, 8; fragmentor, 135; gas temperature, 325 °C; sheath
798 temperature, 325 °C; sheath flow, 11; nebulizer, 40.
799
800 *Metabolome data analysis*
801 The raw data obtained by LC–MS analysis were first converted into mzML format with
802 ProteoWizard software. Peak extraction, alignment, and retention time correction were carried
803 out with the XCMS program, while the peak area was corrected using the "SVR" method. Peaks
804 with a deletion rate of > 50% were filtered out in each group of samples. Next, metabolic
805 identification information was obtained by searching the laboratory's in-house-built database and
806 integrating the public database and the metDNA tool. Finally, statistical analysis was carried out
807 using an in-house-developed R script in RStudio software (v.2021.09.1, R version 4.1.2).
808 Metabolites at the MS2 confidence level were selected for the following analysis. Principal
809 component analysis (PCA) was performed and the results were visualized using the vegan
810 (v.2.5–7) and ggplot2 (v.3.3.5) packages, respectively. Orthogonal partial least squares
811 discriminant analysis (OPLS-DA) was carried out using the ropls (v.1.26.0) package, and
812 metabolites with a VIP > 1, $p < 0.05$, and $|\log FC| > 1$ were identified as differentially abundant

813 metabolites. The abundances of the differentially abundant metabolites in each group were
814 visualized using the ComplexHeatmap (v.2.10.0) package. Spearman correlation analysis was
815 performed on the the metabolome and microbiome data, and the results were visualized using the
816 WGCNA (v.1.70-3) and pheatmap (v.1.0.12) packages, respectively. The Mantel test was
817 performed between the metabolome and microbiome data using the ggcor (v.0.9.4.3) package.
818
819 ***Transcriptome analysis***
820
821 *RNA-seq library construction and sequencing*
822 Total RNA from the colonic epithelial tissue of colitis model mice was extracted using TRIzol
823 reagent (Invitrogen, America). The RNA-seq libraries were constructed using a TruSeq RNA
824 Sample Prep Kit (Illumina, America) according to the manufacturer's instructions. The polyA+
825 RNA was enriched, fragmented, and reverse transcribed to obtain cDNA, and end repair, PCR
826 amplification, purification, and quantification were then performed. The libraries were
827 subsequently sequenced on the Illumina NovaSeq 6000 platform.
828
829 *RNA-seq data analysis*
830 The raw data were quality filtered using fastx_toolkit (v.0.0.14), mapped to the mouse genome
831 GRCm39 using Bowtie2 (v.2.4.1), assembled with cufflinks (v.2.2.1), and quantified with RSEM
832 (v.1.1.3).

833 The transcripts per million (TPM) values were used in the following analysis. Low-abundance
834 data were filtered based on the mean TPM values. The differentially expressed genes were
835 defined as those whose p value was <0.05 with the DESeq2 (v.1.34.0) package, and GO and
836 KEGG enrichment analyses were then performed with the clusterProfiler (v.4.2.1) package. The
837 results were visualized using the ggplot2 (v.3.3.5) and ComplexHeatmap (v.2.10.0) packages.
838
839 ***Cell culture***
840 All the cells were maintained at 37 °C in 5% CO_2 in a Heracell 150i incubator (Thermo Fisher
841 Scientific, America). Human NCM460 cells (ATCC) were cultured in RPMI 1640 medium
842 (Gibco, America) supplemented with 10% fetal bovine serum (Gemini, America). Mouse
843 RAW264.7 cells (ATCC) were cultured in DMEM (Gibco, America) supplemented with 10%
844 fetal bovine serum.
845 To assess the anti-inflammatory effects of the HP derivatives, RAW264.7 cells were seeded in
846 96-well plates, stimulated with 100 ng/ml lipopolysaccharide (Sigma–Aldrich, America) for 15
847 min, and treated with the HP derivatives at a concentration of 1 mg/ml for 24 hr. The
848 supernatants were collected and subjected to ELISA.
849
850 ***UC organoid culture***
851 Human UC patient-derived colonoids were cultured as previously described[40,41] with slight
852 modifications. Colon tissue samples were obtained from biopsies taken from male and female

853 UC patients aged 20 to 80 years (inclusive); in all patients, UC had been clearly diagnosed for
854 more than 3 months through clinical manifestations and endoscopic examination. All samples
855 were graded as mild to moderate active ulcerative colitis (Mayo score: 3–10) and were collected
856 at Tsinghua Changgung Hospital (22111–4-02) in Beijing, washed in ice-cold PBS, incubated
857 with 10 mM DTT for 15 min, and disassociated in PBS containing 20 mM EDTA for 60 min at
858 4 °C. The crypts were isolated by vortexing, collected by centrifugation, embedded in growth
859 factor-reduced Matrigel (Corning), and cultured in complete medium consisting of advanced
860 DMEM/F12 (Thermo Fisher Scientific, America) supplemented with 1% penicillin and
861 streptomycin (Thermo Fisher Scientific, America), 10 mM HEPES (Thermo Fisher Scientific,
862 America), 2 mM GlutaMAX (Thermo Fisher Scientific, America), 1 × B-27 supplement (Thermo
863 Fisher Scientific, America), 1 mM N-acetylcysteine (Sigma–Aldrich, America), 100 ng/ml
864 recombinant mouse EGF (Thermo Fisher Scientific, America), 100 ng/ml recombinant human
865 Noggin (PeproTech, America), 1 μg/ml recombinant human R-spondin-1 (PeproTech, America),
866 500 nM A83-01 (Tocris, England), 10 μM SB202190 (Sigma–Aldrich, America) and 10%
867 Afamin/WNT3A conditioned medium (JSR Life Sciences, Japan). To prevent anoikis, 10 mM Y-
868 27632 (STEMCELL Technologies, Canada) was added to the complete medium for the first day
869 of culture. The colonoids were passaged every 6 to 7 days by mechanical disassociation, and the
870 medium was changed every day to ensure their rapid growth.
871
872 ***EdU labeling***

873 EdU labeling of proliferating cells in the colonic epithelia of colitis model mice was performed
874 on 3-μm sections of paraffin-embedded tissues with a Click-iT EdU Imaging Kit (Invitrogen,
875 America) according to the manufacturer's protocol.
876
877 ***Immunohistochemical and immunofluorescence staining***
878 Paraffin-embedded sections (3 μm thick) were deparaffinized, washed with PBS containing
879 0.01% Tween 20, and subjected to antigen retrieval by immersion in Tris-EDTA buffer (pH 9.0)
880 at 100 °C for 20 min.
881 For immunohistochemical staining, the samples were blocked using peroxidase-blocking
882 solution (Dako, Denmark) and incubated with specific primary antibodies at 4 °C overnight. The
883 fluorescence signals were detected using a REAL EnVision Detection System (Dako, Denmark)
884 and observed using AxioScan. Z1 Slide Scanner (Zeiss, Germay).
885 For immunofluorescence staining, the samples were blocked with 1% BSA/PBS for 1 hr,
886 incubated with specific primary antibodies at 4 °C overnight, and then incubated with secondary
887 antibodies; nuclei were then stained, and the samples were mounted with ProLong Gold Antifade
888 Mountant (Thermo Fisher Scientific, America) and observed using inverted confocal microscopy
889 (Nikon, Japan).
890
891 ***Single-cell RNA sequencing***[42]
892

893 *Preparation of single-cell suspensions from UC organoids*

894 The UC organoids grown on filter paper were placed on an ice-cold plate and allowed to cool for
895 2–3 minutes. The sample wells containing the tissue spheroids to be analyzed were confirmed,
896 the culture medium in the wells was discarded, and the solid Matrigel^{TM} was left. One milliliter
897 of precooled (4 °C) advanced DMEM/F12 culture medium supplemented with 1% HEPES, 1%
898 P/S and 1% GlutaMAX was added to each well, the Matrigel^{TM} surrounding the UC organoids
899 was gently disrupted by pipetting to break it down and dissolve it, and the organoids were
900 collected in 15 mL centrifuge tubes. This procedure was repeated 3 times until all the tissue
901 spheroids were disrupted by pipetting and collected. The mixture was centrifuged at 300 × g and
902 4 °C for 5 minutes, the supernatant was removed, 3 mL of precooled (4 °C) advanced
903 DMEM/F12 culture medium was added to resuspend the pellet, and the mixture was centrifuged
904 again at 200 × g and 4 °C for 5 minutes to remove the supernatant to obtain the colon tissue
905 spheroids. Two milliliters of 0.25% trypsin was added to the suspension, which was subsequently
906 incubated at 37 °C in a water bath for 5 minutes, after which an equal volume of RPMI-1640
907 medium containing 10% fetal bovine serum (FBS) was added to terminate the enzymatic
908 digestion. A 1 mL pipet was used to pipet the suspension ten times. The suspension was
909 centrifuged at 300 × g and 4 °C for 5 minutes, and the supernatant was removed. Then, 2 mL of
910 0.0005% Y-27632/TrypLE was added to generate a suspension, which was incubated at 37 °C in
911 a water bath for 15 minutes and pipetted ten times at 5-minute intervals. After the incubation was
912 complete, an equal volume of RPMI-1640 medium containing 10% FBS was added to terminate

913 the reaction. The suspension was centrifuged at 400 × g and 4 °C for 5 minutes, and the
914 supernatant was removed. Then, 50–200 μL of RPMI-1640 medium containing 10% FBS was
915 added to generate a suspension so that the cell concentration was within the range of 700–1200
916 cells/μL. This suspension was disrupted by vigorous pipetting ten to twenty times to obtain
917 single cells from the UC organoids.
918
919 *Single-cell RNA sequencing and library construction for colonic organoids*
920 The concentration and viability of the cells in the single-cell suspensions of colonic organoids
921 were measured with a cell counter. Samples with a cell viability greater than 80%, an
922 agglomeration rate of less than 5% and a lack of obvious cell debris or impurities were
923 considered suitable for library construction. Using microfluidic technology, gel beads and
924 individual cells with specific cell barcodes and reverse transcription information were coated
925 with oil droplets. The cells were solubilized and released mRNA in this system, and the mRNA
926 was captured by the gel beads and reverse transcribed to generate the full-length cDNA
927 sequence. The oil droplets were then disrupted and purified, the amount of cDNA was increased
928 by PCR amplification, and the sequencing primers were ligated. The cDNA was cleaved into
929 fragments of approximately 200~300 bp by a chemical method, end repair was carried out, P7
930 adapters were connected, sample barcodes were introduced, and the sequence fragments were
931 screened. The library was sequenced on the Illumina NovaSeq platform with a PE150
932 sequencing strategy.

933 The unique molecular identifiers (UMIs) in the off-machine data were preprocessed using
934 CellRanger software, an official tool of 10x Genomics. Loupe Browser 6 software, an official
935 tool of 10x Genomics, was used to delete the multicell data, low-quality data, and apoptotic cell
936 data. The corresponding data barcode criteria were a UMI count of greater than 60,000, a feature
937 count of less than 210, and a percentage of mitochondrial UMIs of greater than 25%. Afterward,
938 the uniform manifold approximation and projection (UMAP) method was used for
939 dimensionality reduction. After dimensionality reduction, the CellRanger off-machine data were
940 imported into R Studio, and Seurat was used for dimensionality reduction classification.
941
942 **Data availability**
943 All the data supporting the results of this study are available within the paper and its
944 Supplementary Materials. Additional processed data are available from the corresponding
945 authors upon request.
946
947 **Methods references**
948 40. Fujii, M., Matano, M., Nanki, K. & Sato, T. Efficient genetic engineering of human
949 intestinal organoids using electroporation. *Nat. Protoc.* **10**, 1474–1485 (2015).
950 41. Sato, T. et al. Long-term expansion of epithelial organoids from human colon, adenoma,
951 adenocarcinoma, and Barrett's epithelium. *Gastroenterology* **141**, 1762–1772 (2011).
952 42. Hao, Y. et al. Dictionary learning for integrative, multimodal and scalable single-cell

analysis. *Nat. Biotechnol.* **42**, 293–304 (2024).

Acknowledgments

We thank the National Center for Electron Microscopy in Beijing, School of Materials Science, Tsinghua University, for assistance with electron microscopy imaging; the Laboratory Animal Resources Center, Tsinghua University, for technical support; and the Center of Biomedical Analysis, Tsinghua University, for assistance with imaging technology and flow cytometry; Key Research and Development Program of the Ministry of Science and Technology (2023YFA0914300) and Shenzhen Medical Research Fund (SMRF, B2302009), for regarding financial assistance.

Author contributions

XH. X., Y. W. and X. J. oversaw the research. W. H., L. H., Y. W., W. Z. and XH. X. designed the research strategy. W. H., XY. R and W. Z. established the ulcerative colitis organoids. W. H., L. H., ZK. L., QX. Z., W. Z, and XY. R. performed the experiments. W. H., Y. W., and ZQ. Z. analyzed the experimental data. W. H., Y. W., and XH. X. prepared the manuscript. YS. Y., HC. Z and Y. C. provided the materials needed for the experiments. All the authors approved the manuscript.

Competing interests

XH. X., W. H. and Y. W. are inventors on related patents filed by Tsinghua University describing the materials reported in this study. The other authors declare that they have no competing

interests.

978 **Extended Data**

979 **Extended Data Fig.1| Therapeutic efficacy evaluation of the library of non-anticoagulated**

980 **heparin derivatives.**

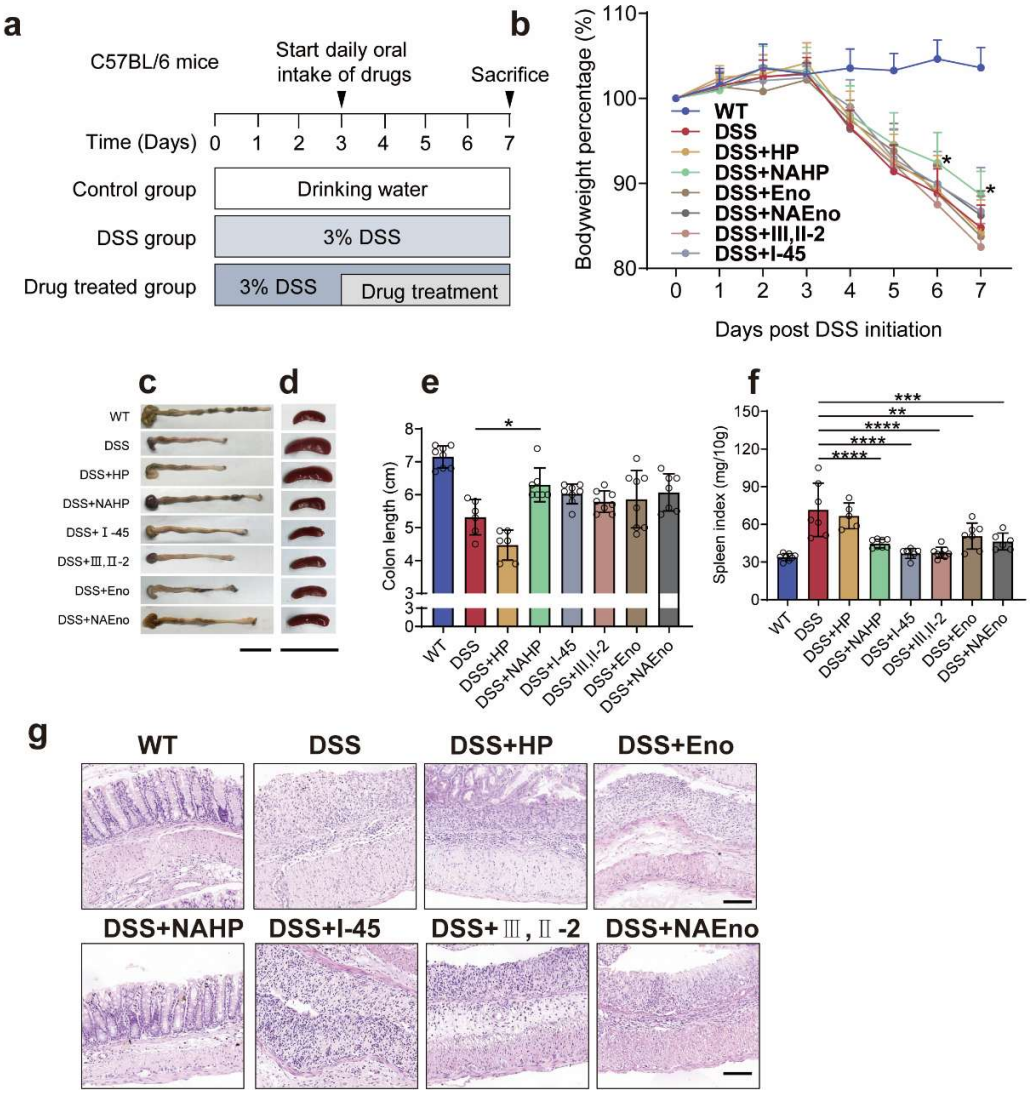

981

982 **a,** 3%DSS was added to the drinking water for 7 days to induce acute colitis in mice (n=10). The

983 control group of mice was given regular drinking water (n=10), and the drug treatment group was

984 given 30mg/kg heparin (HP), Enoxaparin (Eno), Nonanticoagulant heparin (NAHP),

985 Nonanticoagulant Enoxaparin (NAEno), Heparin digested by heparinase I(I-45), Heparin digested
986 by heparinase II and heparinase III(III-II-2) on the third day (n=10). **b,** Changes in weight **c-f,** Mice
987 were scarified on day 7 and colon (**c**) and spleen (**d**) were collected, Colon length (**e**) and Spleen
988 index (**f**) were quantitated. **g,** Representative images of colons stained with Hematoxylin and eosin,
989 Scale bar, 100μm. Shown (**b, e, f**) are representative images or quantitative analysis from at least
990 n=5 biologically independent samples. Data represent mean ±SD. * $p < 0.05$, ** $p < 0.01$, *** $p <$
991 0.001, **** $p < 0.0001$ and ns (no significance) $p > 0.05$, analyzed by ordinary one-way ANOVA
992 (**b**) multiple comparisons test.
993

Extended Data Fig.2| Therapeutic efficacy evaluation of different molecular weight NAHP.

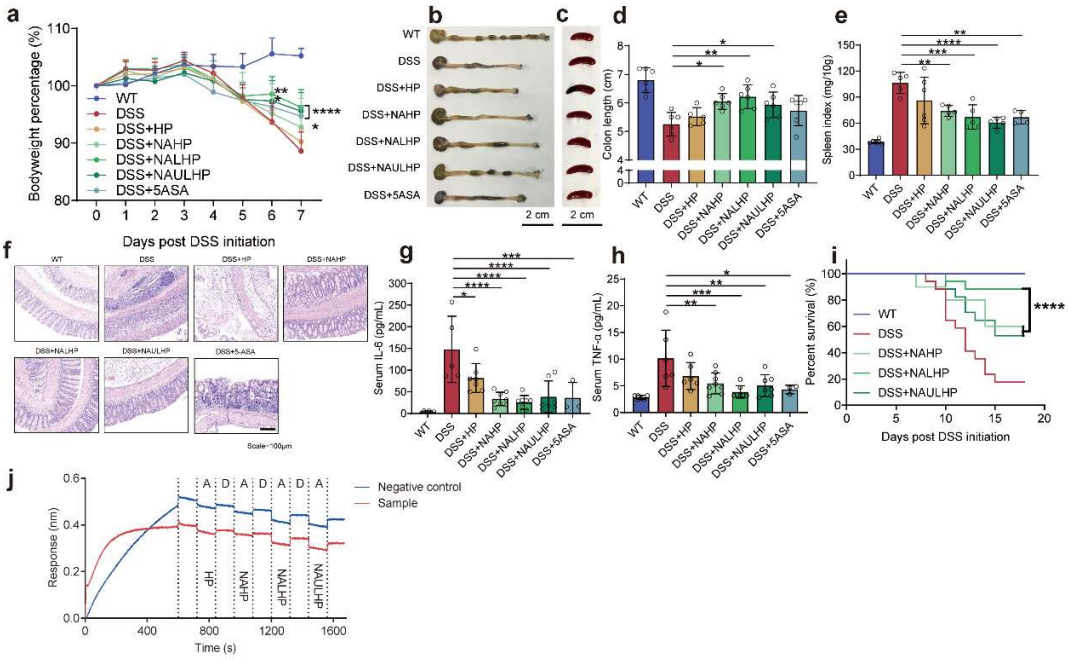

a, Changes in weight **b-e,** Mice were scarified on day 7 and colon (**b**) and spleen (**c**) were collected, Colon length (**d**) and Spleen index (**e**) were quantitated. **f,** Representative images of colons stained with Hematoxylin and eosin, Scale bar, 100μm. **g,h,** The concentration of Serum IL-6 (**g**) and TNF-α (**h**) were determined by ELISA when mice were scarified on day 7. **i,** The death status of mice after being modeled with DSS and treated with NAHP, NALHP and NAULHP. **j,** The adsorption(A) and desorption(D) response curves among HP, NAHP, NALHP, NAULHP and DSS by Bio-Layer Interferometry (BLI), blue line represents the blank contrast, orange line represents the sample.

Shown (**a, d, e, g-l**) are representative images or quantitative analysis from at least n=5 biologically independent samples. Data represent mean ±SD. * $p < 0.05$, ** $p < 0.01$, *** $p < 0.001$, **** $p <$

1006 0.0001 and ns (no significance) $p > 0.05$, analyzed by ordinary one-way ANOVA (**a**) multiple

1007 comparisons test.

1008

Extended Data Fig. 3| The physicochemical properties of heparin derivatives.

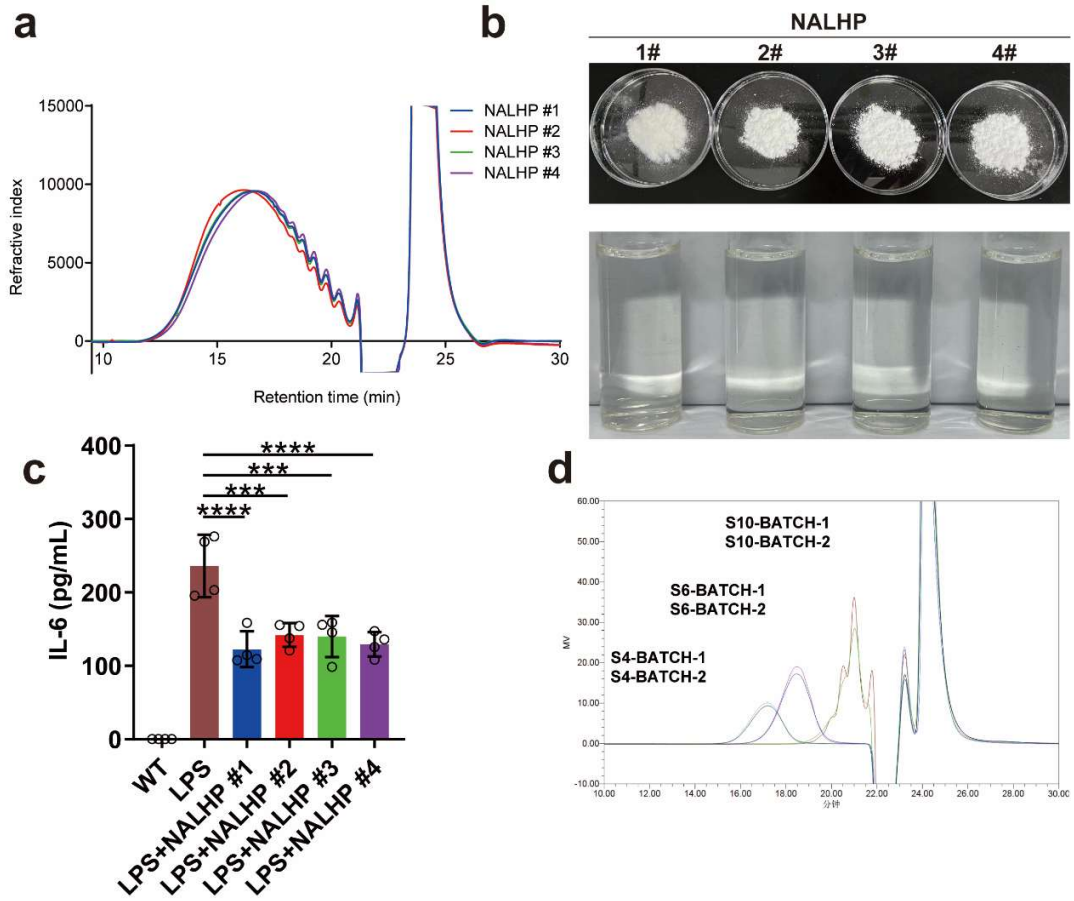

a, Gel chromatograms of four batches production of NALHP. **b,** The morphology and solubility of NALHP prepared by four batches (#1-#4). **c,** The concentration of IL-6 factor in the cell supernatant of RAW264.7 cells after treatment with the four batches of NALHP. **d**, Gel exclusion chromatograms of the separated components from two batches (BATCH-1 and -2). Shown (**c**) are representative images or quantitative analysis from n=4 biologically independent samples. Data represent mean ±SD. * $p < 0.05$, ** $p < 0.01$, *** $p < 0.001$, **** $p < 0.0001$ and ns (no significance) $p > 0.05$, analyzed by ordinary one-way ANOVA (**g**) multiple comparisons test.

Extended Data Fig.4 | Therapeutic efficacy evaluation of different non-anticoagulated heparin derivates.

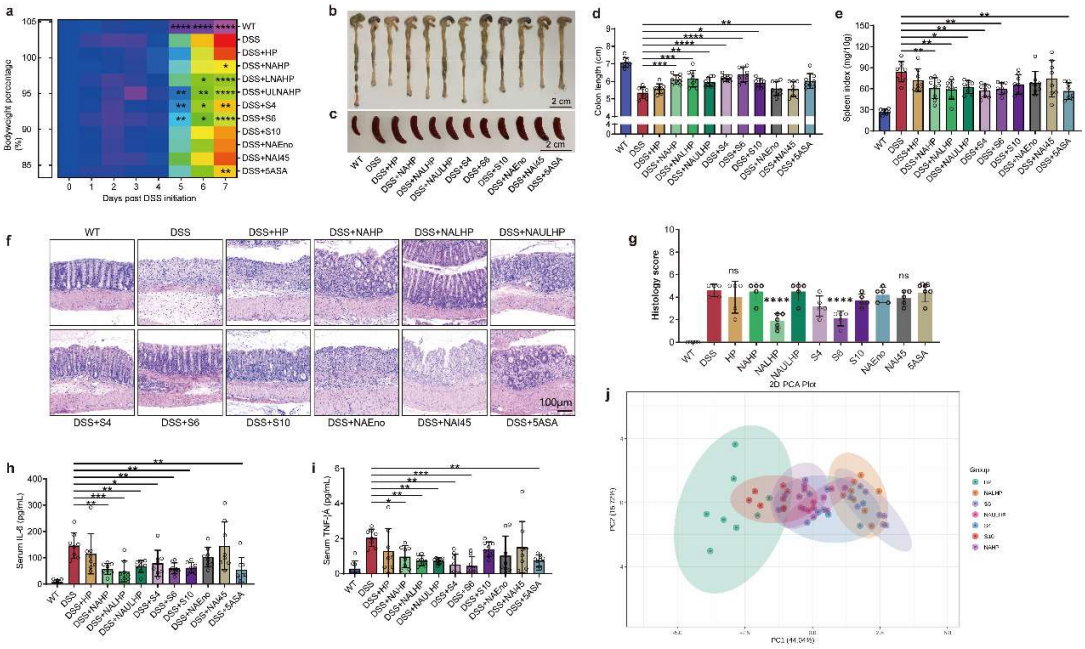

a, Changes in weight. **b-e,** Mice were scarified on day 7 and colon (**b**) and spleen (**c**) were collected, Colon length (**d**) and Spleen index (**e**) were quantitated. **f,** Representative images of colons stained with Hematoxylin and eosin, and Histological score (**g**) were quantified. Scale, 100μm. **h,i,** The concentration of Serum IL-6 (**h**) and TNF-α (**i**) were determined by ELISA when mice were scarified on day 7. j, Principal component analysis of phenotypes pertaining to UC treatment by HP, NAHP, NALHP, NAULHP, S4, S6 and S10.

Shown (**d, e, g-i**) are representative images or quantitative analysis from n=6 biologically independent samples. Data represent mean ±SD. * $p < 0.05$, ** $p < 0.01$, *** $p < 0.001$, **** $p < 0.0001$ and ns (no significance) $p > 0.05$, analyzed by ordinary one-way ANOVA (**a**) multiple comparisons test. The data obtained from the PCA analysis represent the improvement in the

1032 characteristics of UC mice (including body weight, colon length, spleen index, serum IL-6 and

1033 TNF-α levels, and histological scores) treated with drugs of different molecular weights (HP,

1034 NAHP, NALHP, NAULHP, S4, S6 and S10).

1035

1036

Extended Data Table.1 The molecular weight size and distribution of NALHP and its fine fragments

Name	Separation(mg)	Content (%, w/w)	M_w （Da）	P	M_w（Da）Distribution（%）			
					>8k	5k~8k	3k~5k	<3k
NALHP	650	100	6224	2.33	28.04	27.87	19.11	24.95
NAULHP	-	-	2974	3.22	5.21	14.96	20.05	59.77
S1	37.7	5.8	12121	1.036	99	1		
S2	44.2	6.8	9557	1.037	80	20		
S3	42.9	6.6	7686	1.038	38	60	2	
S4	37.7	5.8	6254	1.041	8	78	13	
S5	89.7	13.8	5094	1.055	1	50	46	2
S6	99.5	15.3	4115	1.076		19	68	13
S7	71.5	11.0	3227	1.117		5	50	45
S8	78.65	12.1	2426	1.172		1	23	76
S9	62.4	9.6	1736	1.188			7	93
S10	48.1	7.4	1282	1.153			1	99
S11	37.7	5.8	812	1.073				100

Extended Data Fig. 5| Therapeutic efficacy evaluation of the library of S6.

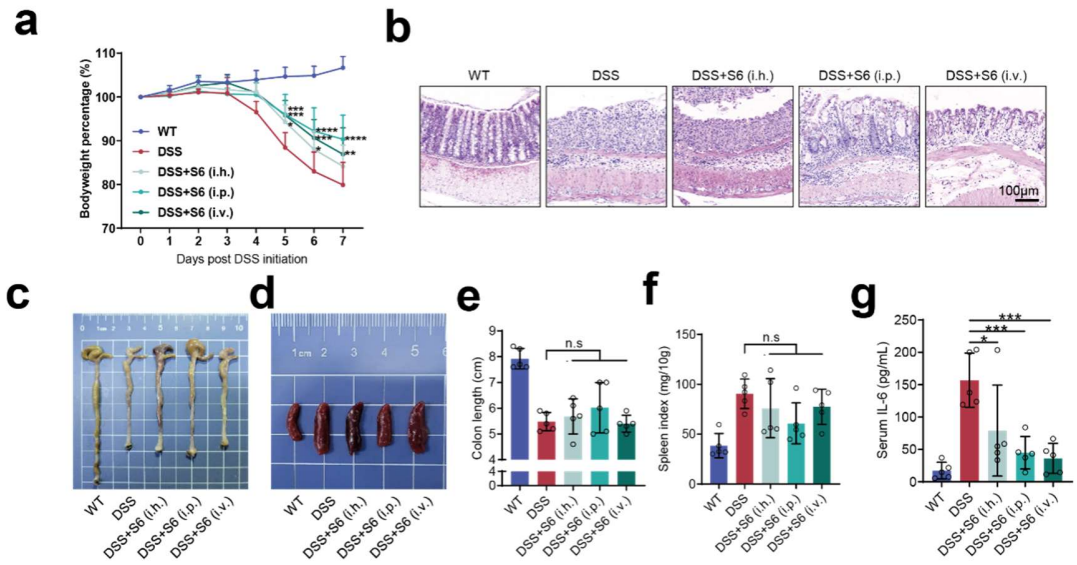

a, The body weight changes of mice under different administration methods (Intravenous injection(i.v.), intraperitoneal injection(i.p.), hypodermic injection(i.h.)). **b,** The body weight changes of mice under different administration methods. **c-f,** Mice were scarified on day 7 and colon (**c**) and spleen (**d**) were collected, Colon length (**e**) and Spleen index (**f**) were quantitated. **g,** The concentration of Serum IL-6 was determined by ELISA when mice were scarified on day 7. Shown (**a, e-g**) are representative images or quantitative analysis from at least n=5 biologically independent samples. Data represent mean ±SD. * $p < 0.05$, ** $p < 0.01$, *** $p < 0.001$, **** $p < 0.0001$ and ns (no significance) $p > 0.05$, analyzed by ordinary one-way ANOVA (**g**) multiple comparisons test.

1056 **Extended Data Fig. 6| Infrared spectra of different heparin derivatives.**

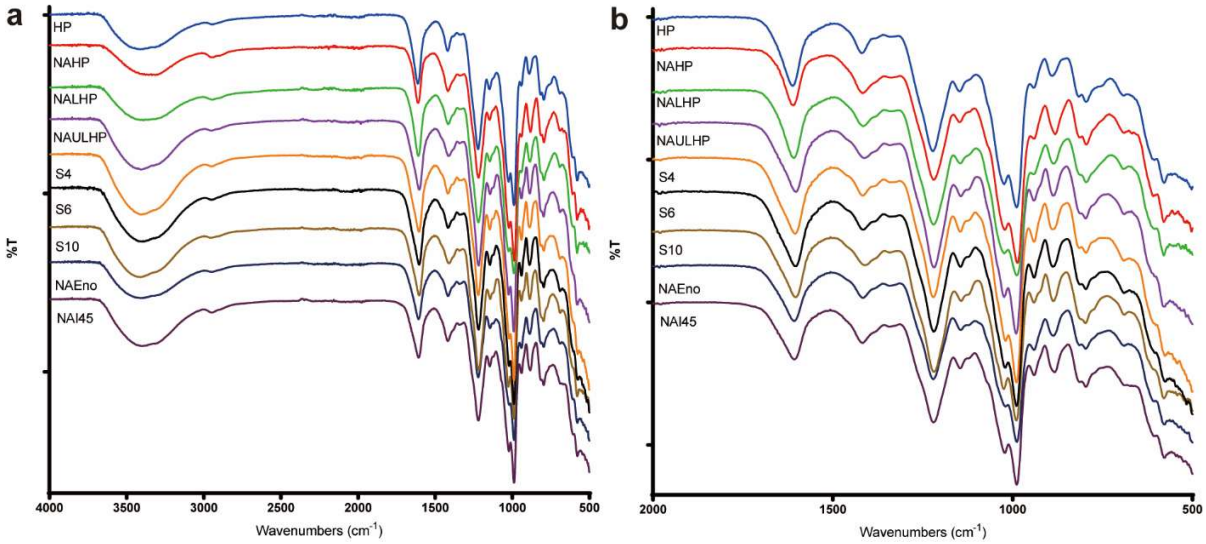

1057

1058 **a,** Infrared full spectrum of heparin derivates. **b,** Infrared spectra between 2000 cm^{-1} and 500 cm^{-}

1059 ^{1} of heparin derivates.

1060

1061

1062

1063

Extended Data Table.2 The batch numbers of raw materials and products of 4 batches of NALHP production

Batch Number	#1	#2	#3	#4
HP	NHS210204	NHS200606	NHS200803	NHS180302
NAHP	BATCH-211019	BATCH-210401	BATCH-210319	BATCH-190304
NALHP	BATCH-211023	BATCH-210408	BATCH-210402	BATCH-190504

Extended Data Table.3 Preparation process parameter standards for 4 batches of NALHP production

Process Indicators	#1	#2	#3	#4	Process standard	Qualified or unqualified
anti-Xa（IU/mg）	19.4	18.1	18.5	19.0	<20	Qualified
A_{232}	19.0	12.2	28.1	23.4	<30	Qualified
ΔA_{232}	41.0	39.7	38.8	39.6	39.5±2.0	Qualified
A_{294}	0.167	0.134	0.189	0.245	<0.350	Qualified
A_{420}	0.018	0.019	0.015	0.022	<0.025	Qualified
NALHP ΔM_w（Da）	102	136	150	242	-300~300	Qualified

Extended Data Table.4 The molecular weight size and distribution of 4 batches of NALHP production

Batch number	M_w（Da）	ΔM_w（Da）	P	M_w（Da）Distribution（%）			
				>8k	5k~8k	3k~5k	<3k
#1	6326	102	1.505	28	34	20	18
#2	6360	136	1.494	29	33	21	17
#3	6374	150	1.573	30	32	19	19
#4	6466	242	1.548	31	29	21	19
Standard	6224	0	1.531	28	32	21	19

1078 **Extended Data Fig.7 | ^{13}C NMR spectrum of different heparin derivatives.**

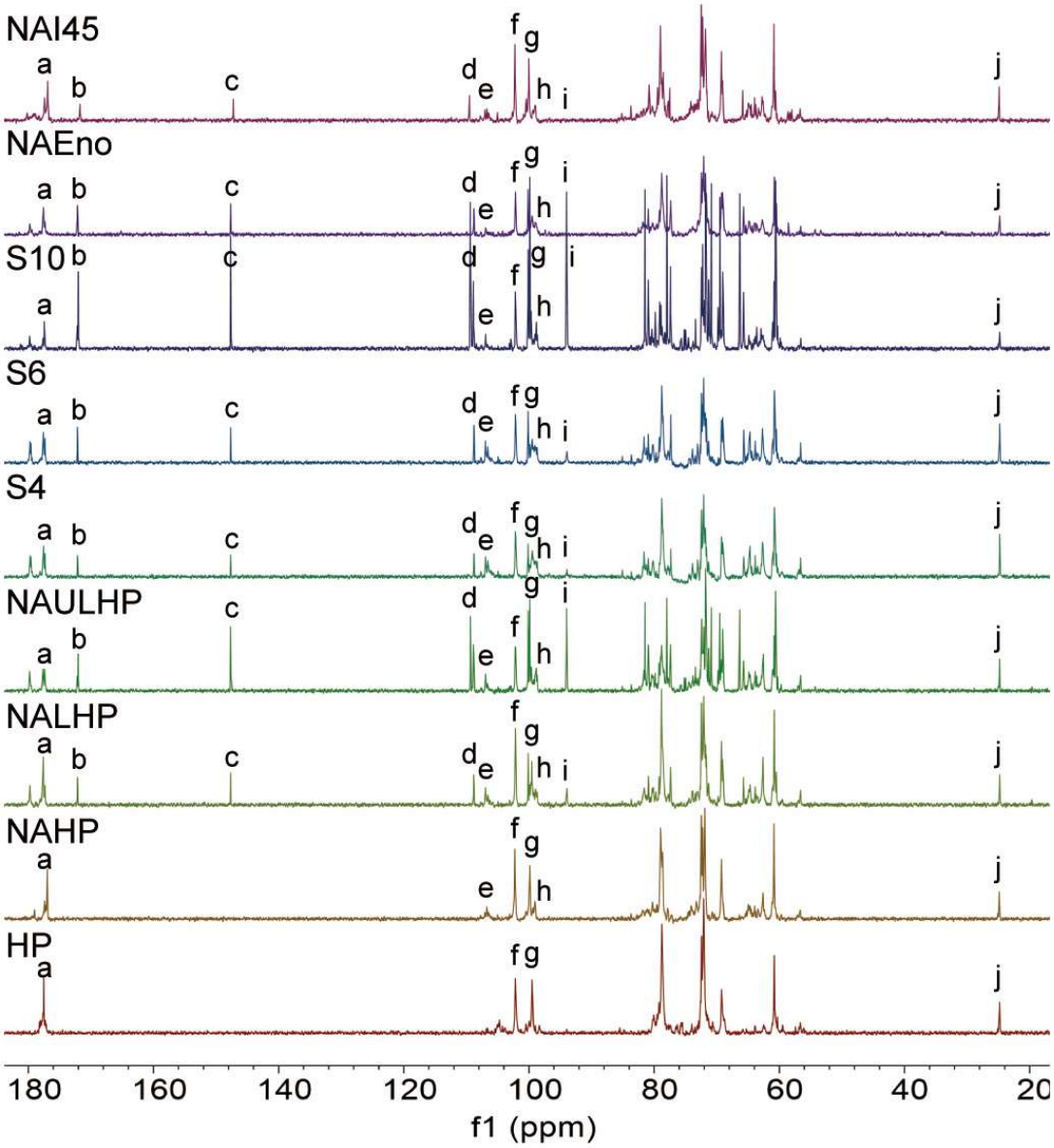

1079

1080

1081 **Extended Data Table.5** ^{13}C NMR chemical shift attribution of HP and different non-
1082 anticoagulated heparin derivatives

Peak position	Test the chemical shift of the sample（ppm）							Chemical shift attribution
	HP	NAHP	NALHP	NAULHP	S4	S6	S10	
a	177.7	176.7	177.7	177.7	177.7	177.7	177.7	U, -**C**OOH; GlcNAc6S / GlcNAc, CH_3**C**O-
b	-	-	172.1	172.1	172.1	172.1	172.1	ΔU / ΔU2S, -**C**OOH
c	-	-	147.6	147.6	147.6	147.6	147.6	ΔU2S, **C5**
d	-	-	108.9	108.9	108.9	108.9	108.9	ΔU2S, **C4**
e	-	106.7	106.7	106.7	106.7	106.7	106.7	gsIdoA / gsGlcA, **C1**
f	102.3	102.3	102.3	102.3	102.3	102.3	102.3	IdoA2S, **C1**
g	99.9	99.9	99.9	99.9	99.9	99.9	99.9	ΔU2S / GlcNS6S / GlcNS / GlcNAc6S / GlcNAc, **C1**
h	-	99.1	99.1	99.1	99.1	99.1	99.1	**GlcNAc**-(gsIdoA)/ **GlcNAc**-(gsGlcA), **C1**
i	-	-	93.9	93.9	93.9	93.9	93.9	GlcNS-α-RE
j	24.8	24.8	24.8	24.8	24.8	24.8	24.8	-**C**H_3CO-

1083

1084

1085

1086

1087

1088

1089 **Extended Data Fig.8| ^{1}H NMR spectrum of different heparin derivatives.**

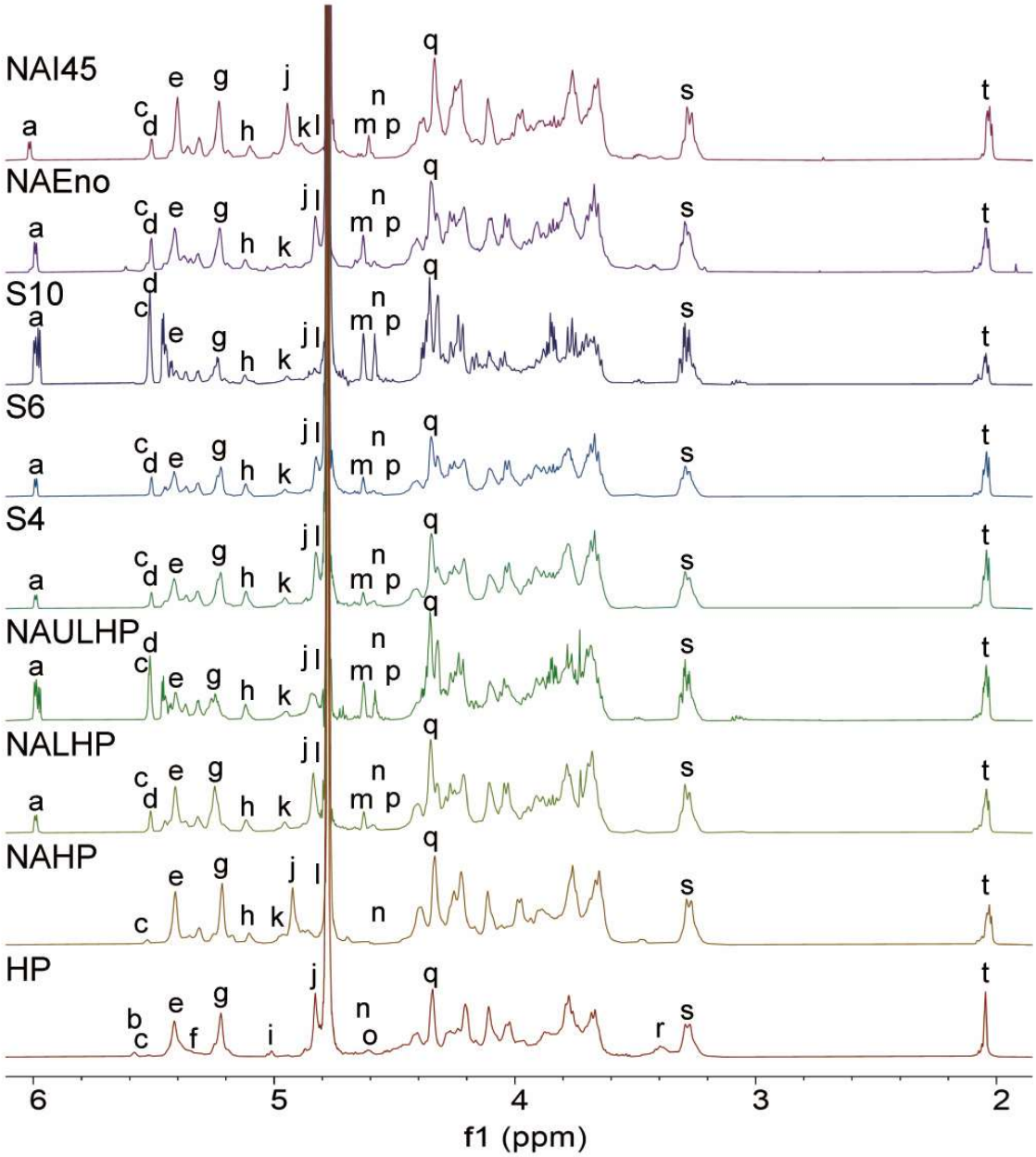

1090

1091

1092 **Extended Data Table.6** ^{1}H NMR chemical shift attribution of HP and different non-
1093 anticoagulated heparin derivatives

Peak position	Test the chemical shift of the sample（ppm）							Chemical shift attribution
	HP	NAHP	NALHP	NAULHP	S4	S6	S10	
a	-	-	5.99	5.99	5.99	5.99	5.99	ΔU, **H4**
b	5.58	-	-	-	-	-	-	**GlcNS**-(GlcA), **H1**
c	5.53	5.53	5.53	5.53	5.53	5.53	5.53	GlcNS3S6S, **H1**
d	-	-	5.52	5.52	5.52	5.52	5.52	ΔU, **H1**
e	5.42	5.42	5.42	5.42	5.42	5.42	5.42	GlcNS6S / GlcNAc6X / **GlcNS6X**-(gsIdoA) / **GlcNS6X**-(gsGlcA), **H1**
f	5.35	-	-	-	-	-	-	**GlcNS6X**-(IdoA), **H1**
g	5.22	5.22	5.22	5.22	5.22	5.22	5.22	IdoA2S, **H1**
h	-	5.12	5.12	5.12	5.12	5.12	5.12	**GlcNAc**-(gsIdoA)/ **GlcNAc**-(gsGlcA), **H1**
i	5.01	-	-	-	-	-	-	**IdoA**-(GlcNS), **H1**
j	4.83	4.92	4.83	4.83	4.83	4.83	4.83	IdoA2S, **H5**
k	-	4.97	4.97	4.97	4.97	4.97	4.97	gsIdoA, **H1**
l	-	4.85	4.85	4.85	4.85	4.85	4.85	gsGlcA, **H1**
m	-	4.73	4.73	4.73	4.73	4.73	4.73	gsXyl, **H1**
n	4.64	4.64	4.64	4.64	4.64	4.64	4.64	Gal, **H1**
o	4.61	-	-	-	-	-	-	GlcA, **H1**
p	-	-	4.63	4.63	4.63	4.63	4.63	ΔU, **H2**
q	4.34	4.34	4.34	4.34	4.34	4.34	4.34	IdoA2S, **H2**
r	3.40	-	-	-	-	-	-	GlcA, **H2**
s	3.28	3.28	3.28	3.28	3.28	3.28	3.28	GlcNS6X, **H2**
t	2.05	2.05	2.05	2.05	2.05	2.05	2.05	-C**H**$_3$CO

1094 **Extended Data Fig.9| Heteronuclear singular quantum correlation (HSQC) of different**

1095 **heparin derivatives.**

1096

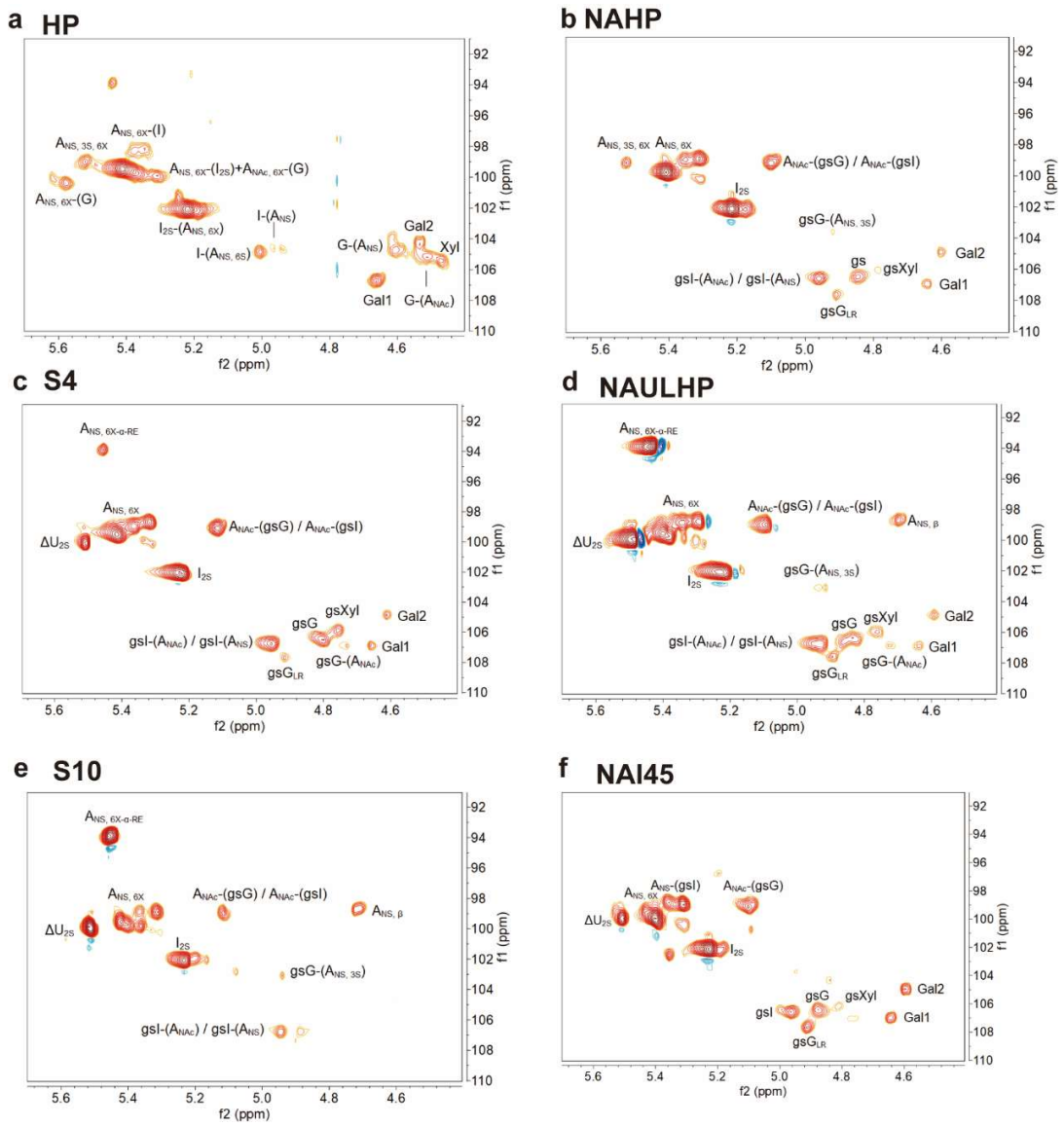

1097

1098 **a,** HP. **b,** NAHP. **c,** S4. **d,** NAULHP**. e,** S10. **f,** NAI45.

1099

1100

Extended Data Fig.10| Microbiological and metabolome analysis.

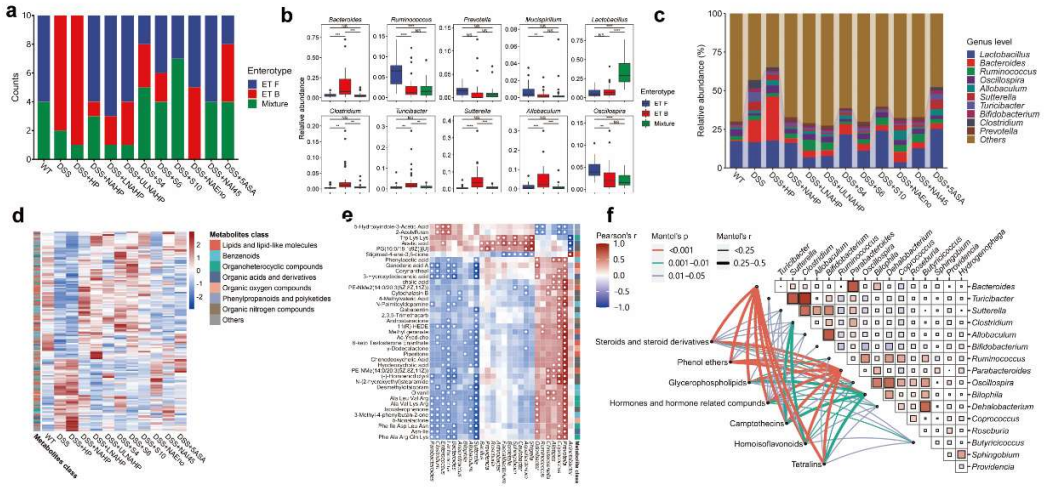

a, Intestinal type analysis under the action of different heparin derivatives. **b,** The distribution of marker flora at the genus level in the DMM classification model. **c,** The composition of intestinal flora at the genus level in each experimental group. **d,** Changes in metabolites among different experimental groups**. e,** Spearman correlation analysis of the microbiome and metabolome. **f,** Mantel analysis of the microbiome and metabolome.

1110 **Extended Data Fig.11| Transcriptome analysis of the colons of UC and drug-treated mice.**

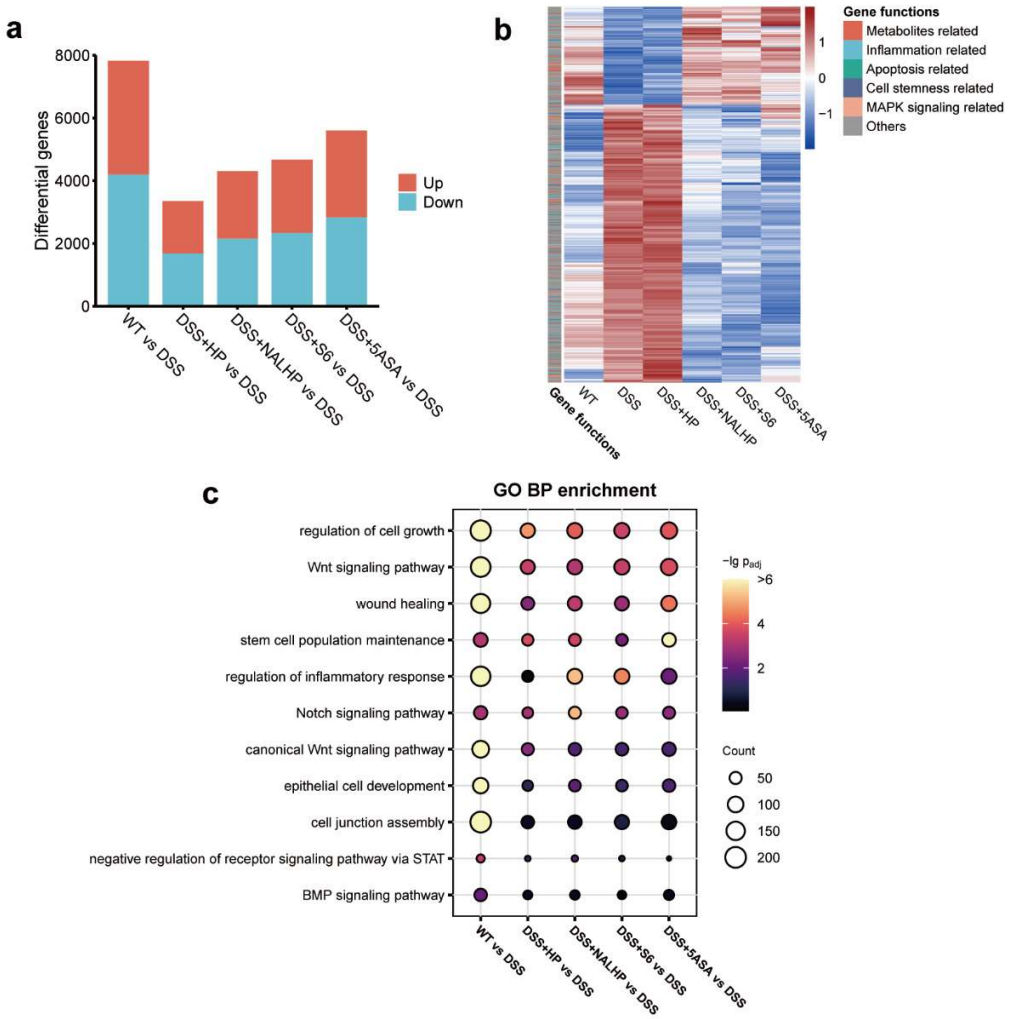

1111

1112 **a,** Differential genes analysis. **b,** Enrichment analysis of differential genes. **c,** GO enrichment

1113 analysis of differential genes under the action of different heparin derivatives.

1114

1115 **Extended Data Fig.12| The expression level of TCF1 in the colonic submucosal layer of**

1116 **colitis model mice.**

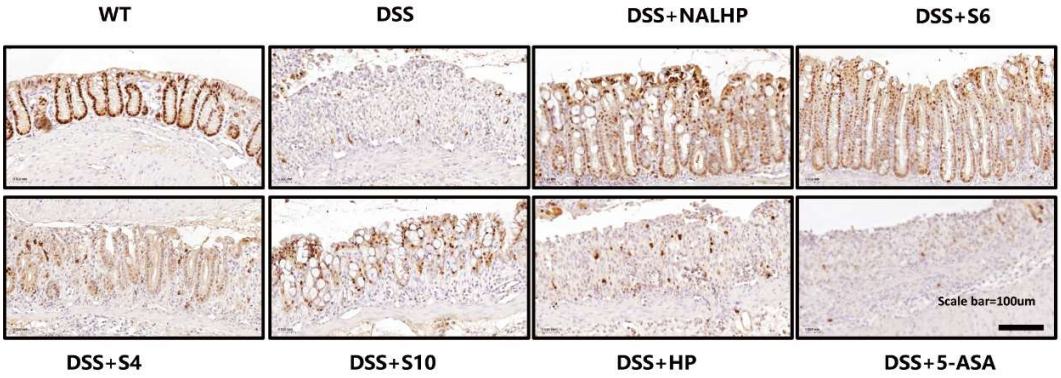

1117

1118 Representative images of immunohistochemical staining for TCF1 in healthy and colitis mice

1119 treated by water, NALHP, S6, S4, S10, HP and 5-ASA. Scale bar, 100 μm. Representative

1120 images from n= 5 biologically independent samples are shown.

1121

1122

1123 **Extended Data Fig.13| The expression level of PCNA in the colonic submucosal layer of**
1124 **colitis model mice.**

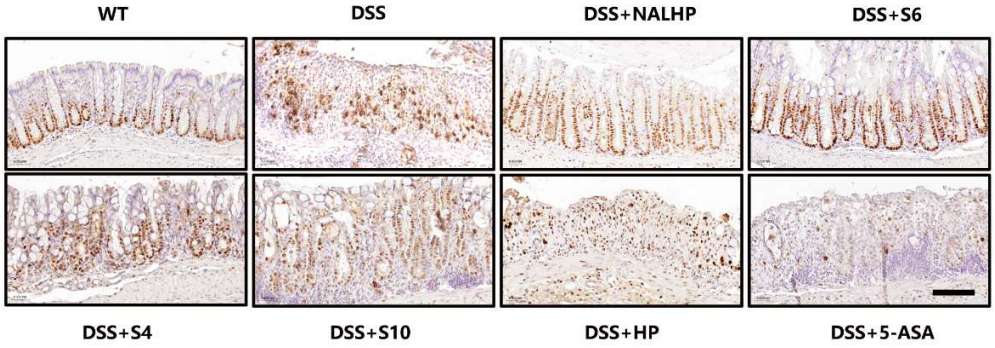

1125

1126 Representative images of immunohistochemical staining for PCNA in healthy and colitis mice

1127 treated by water, NALHP, S6, S4, S10, HP and 5-ASA. Scale bar, 100 μm. Representative

1128 images from n= 5 biologically independent samples are shown.

1129

1130

1131

1132

1133

1134

Extended Data Fig.14| The expression levels of MUC2 and PCNA vary among human [1], mice, and organoids.

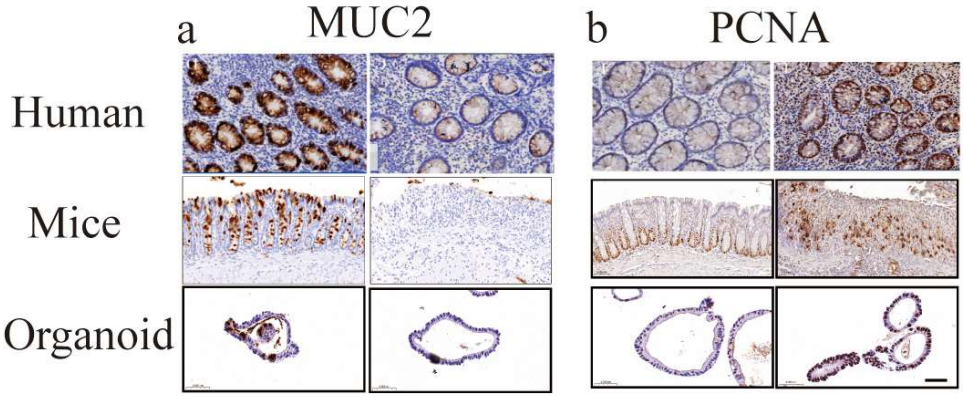

Representative images of immunohistochemical staining for MUC2(a) and PCNA(b) in human, mice and organoids. Scale bar, 50 μm. Representative images from n= 3 biologically independent samples are shown.

[1] He, T., Wang, W., Li, L., Qiu, S., Sun, S., & Zong, L. (2022). PCNA, EGFR, MUC2 expression levels and clinical significance in ulcerative colitis. *Journal of Medical Research*, *51*(3), 104-107.

1148 **Extended Data Fig.15| Single-cell transcriptome analysis.**

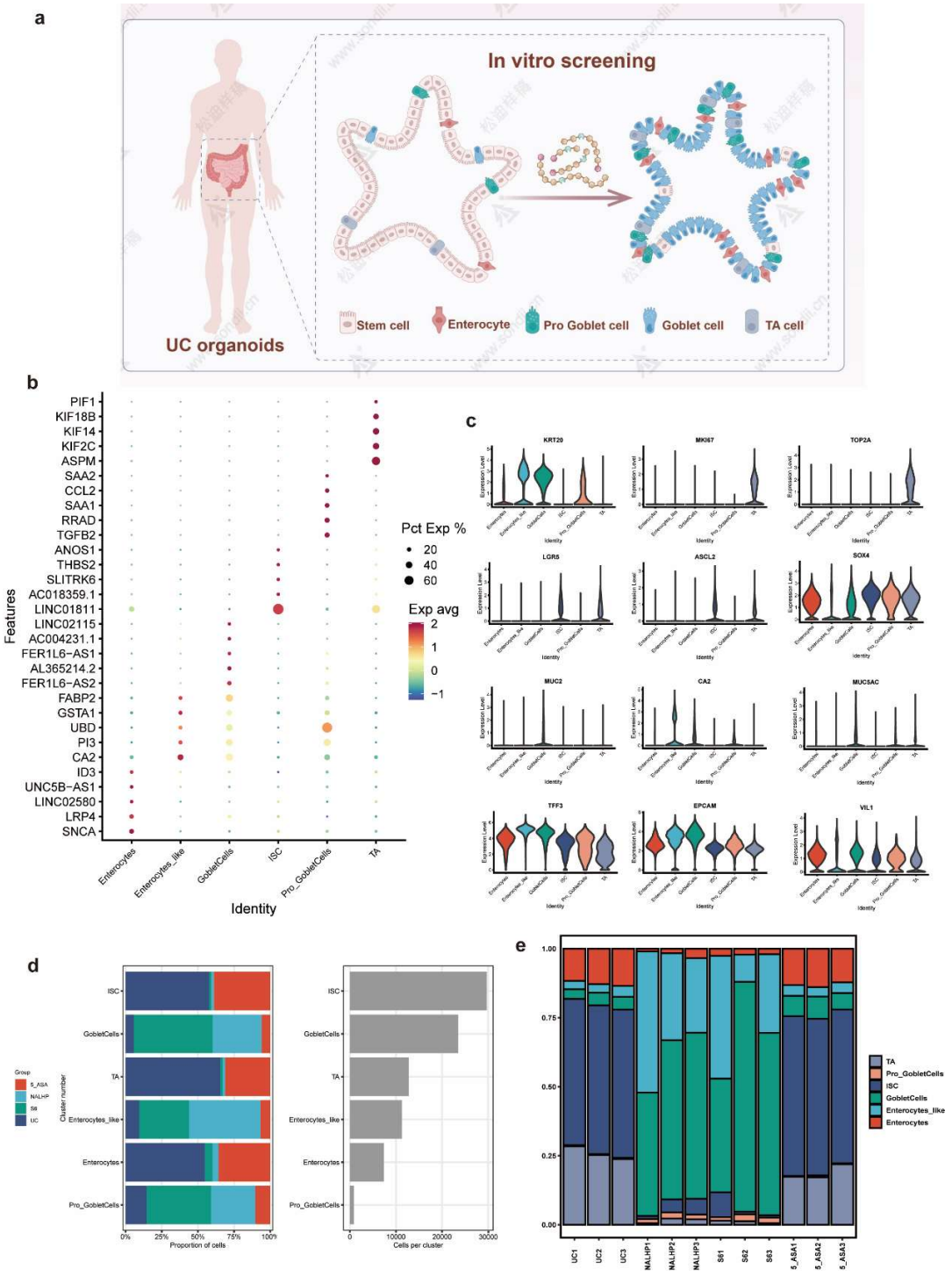

1149

1150 **a,** The proportion of cells in different groups. **b,** The changes in cell types of organoids under the

1151 action of heparin derivatives. **c,** Cell typing criteria. **d,** The expression of genes in different cell

1152 types. **e,** Schematic diagram of cell type changes in UC organoids.

1153

1154

Extended Data Fig.16 | Pseudotime Analysis reveals the trajectory of stem cells differentiating into goblet cells in organoids

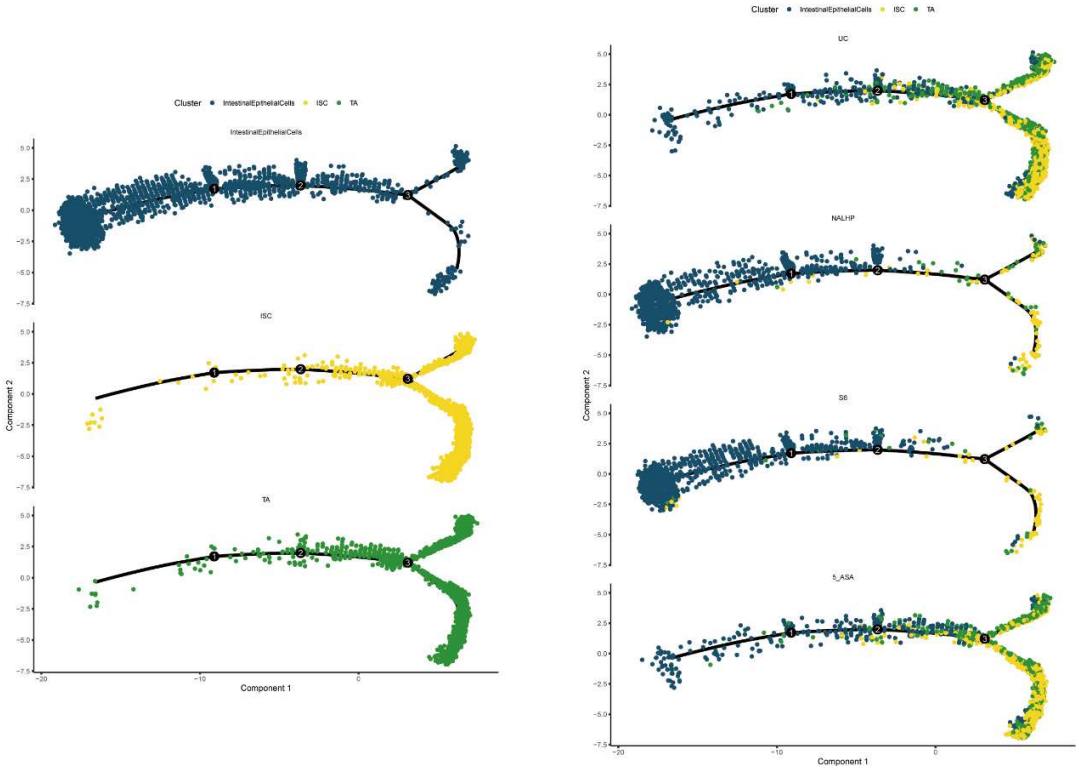

The single-cell RNA-seq data from stem cells of UC-type organs were subjected to time-series analysis (using Monocle2) under different cell types **(a)** and different group **(b)**. The cells were arranged on a continuous trajectory based on their transcriptional status. The cells were sorted according to pseudo-time, and genes were clustered according to their expression patterns (blue: intestinal epithelial cells; yellow: intestinal stem cells; green: TA cells).

Extended Data Fig.17 | U-map dimensionality reduction analysis.

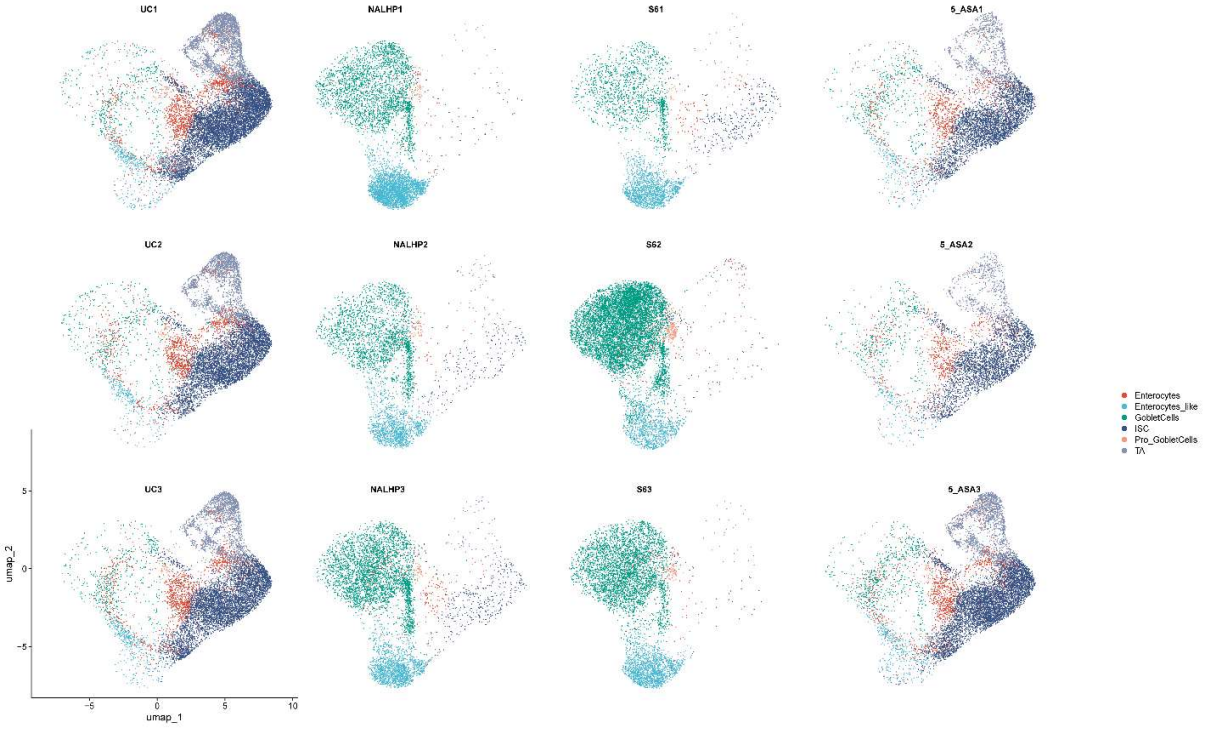

Dimensionality reduction of U-maps under the effects of NALHP, S6, and 5-ASA in three different UC patient derived UC organoids (UC1-UC3).

1175 **Extended Data Fig.18 | NCM460 cell fluorescence staining image**

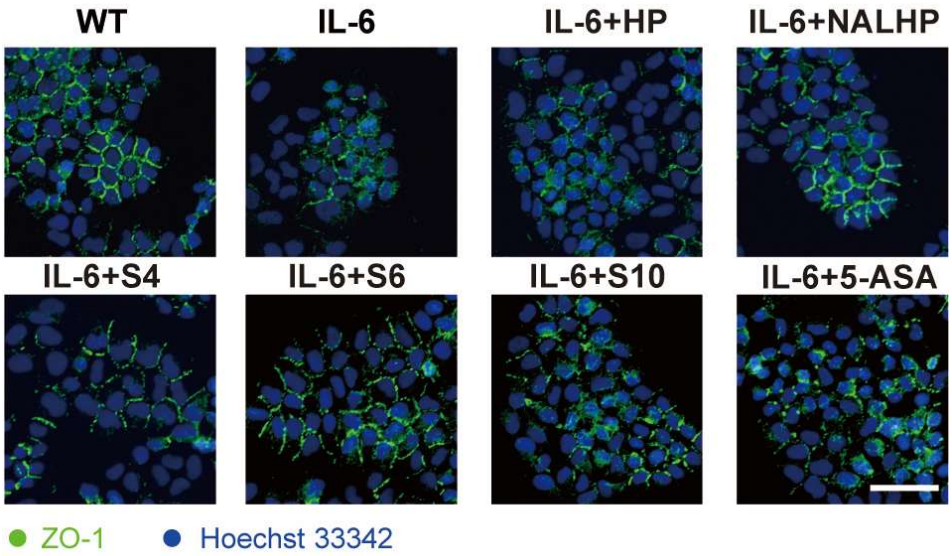

1176

1177 NCM460 cells were stimulated with IL-6 and treated with HP, NALHP, S4, S6, S10, 5-ASA (1

1178 mg/mL), scale bar=50 um. The expression level of ZO-1 protein was detected by fluorescent

1179 staining.

1180

1181 **Extended Data Fig.19 | Organoid transcriptomic analysis.**

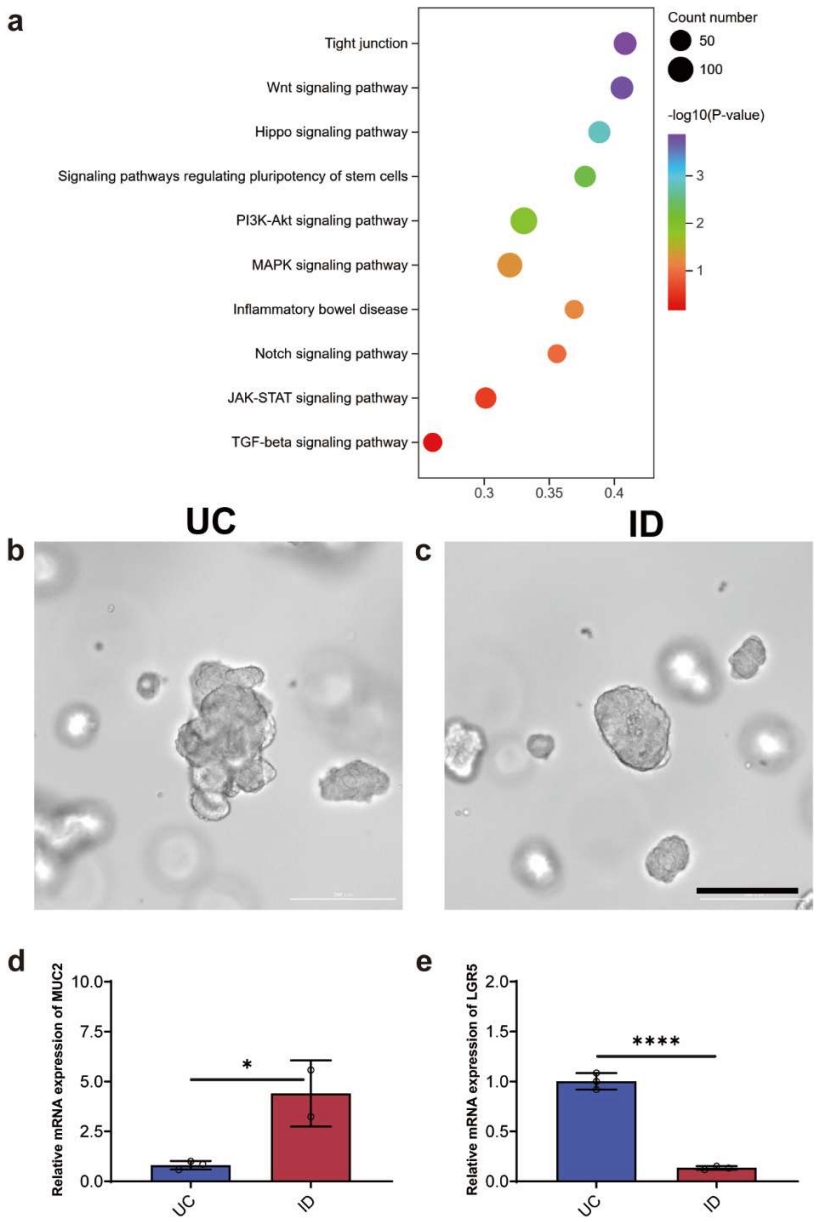

1182

1183 **a,** GO enrichment analysis of differentially expressed genes in UC organoids after NALHP

1184 treatment. **b,c,** Bright-field diagram of untreated (UC)(**b**) and under the treatment of IWP-2 and

1185 DAPT (ID)(**c**), scale bar=200 um. **d,e,** Relative mRNA expression of MUC2(**d**) and LGR5(**e**)

1186 under the treatment of IWP-2 and DAPT (ID).

1187

1188 **Extended Data Fig.20 | Bright-field diagram**

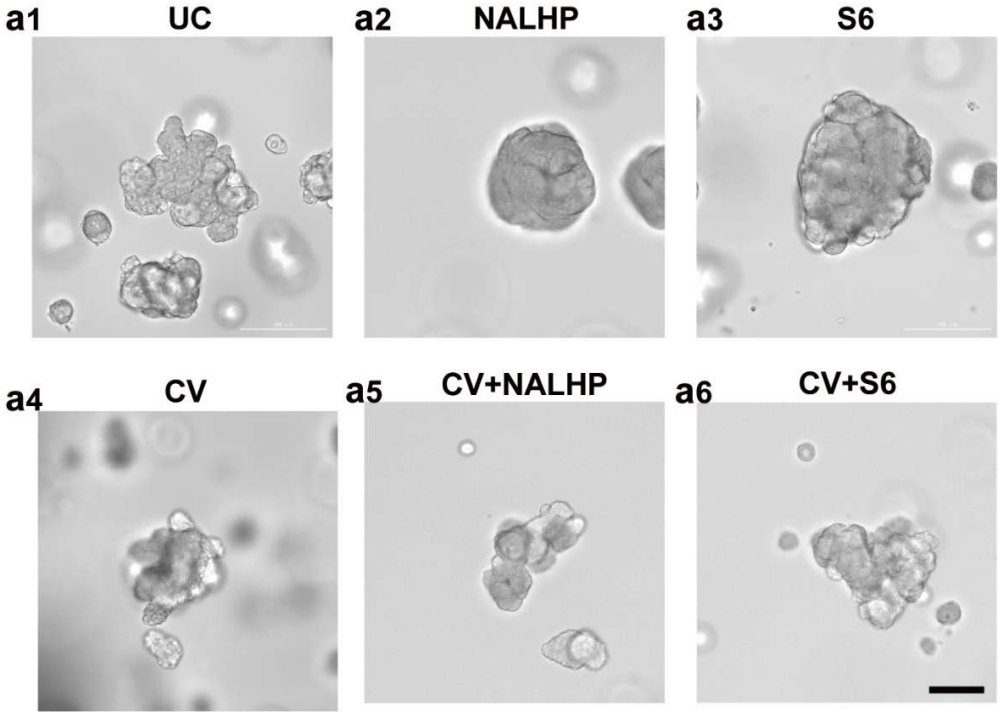

1189

1190

1191 UC organoids under the treatment of NALHP(a2), S6(a3), CV(a4), CV+NALHP(a5),

1192 CV+S6(a6), scale bar=200 um

1193

1194 **Extended Data Fig.21 | Expression of key proteins after NALHP/S6 and CHIR99021(C)**

1195 **and VPA(V) were co-cultured with UC organoids.**

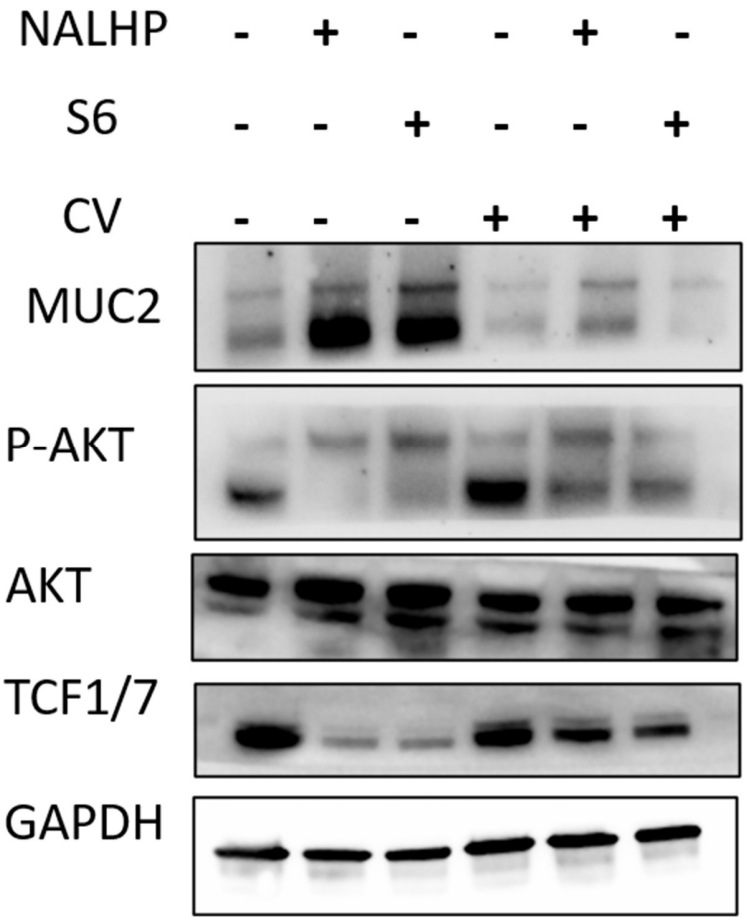

1196

1197

1198

1199

Extended Data Fig.22 | Expression of key proteins after NALHP/S6 and CHIR99021(C) were co-cultured with UC organoids.

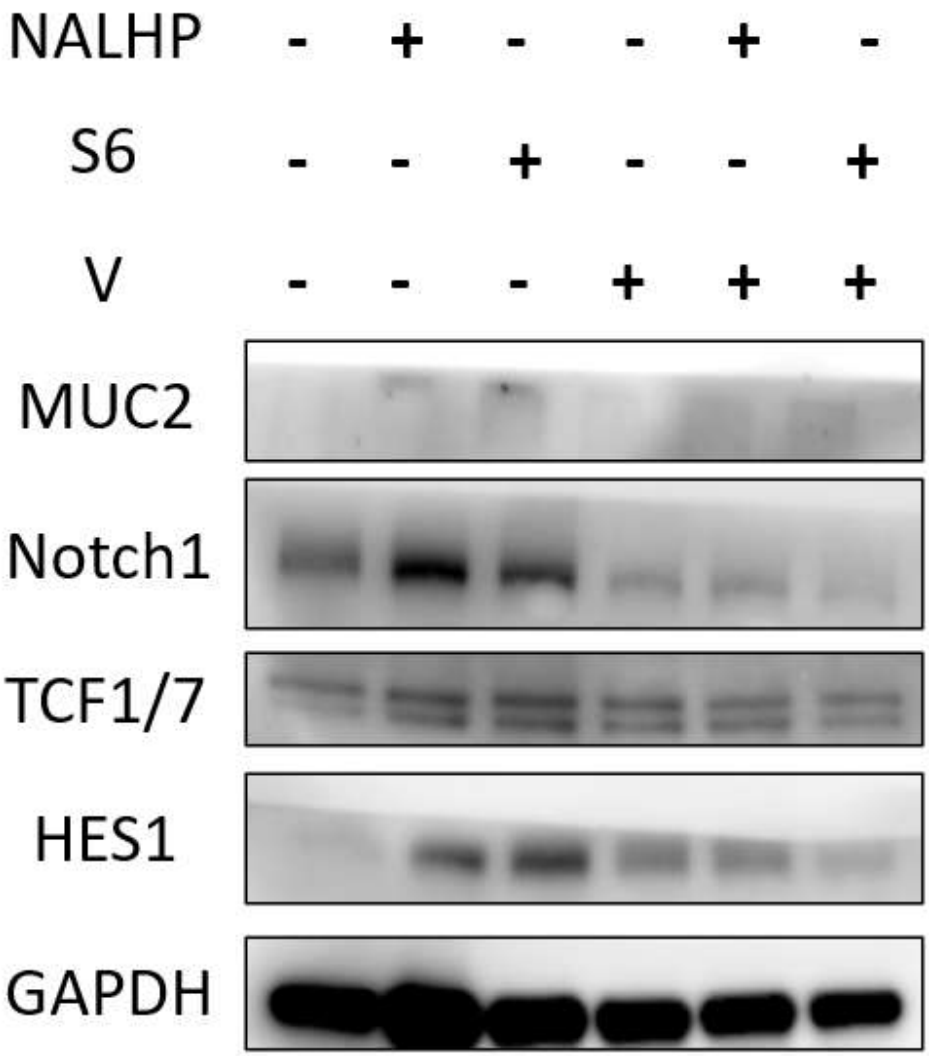

1204 **Extended Data Fig.23 | Expression of key proteins after NALHP/S6 and VPA(V) were co-**

1205 **cultured with UC organoids.**

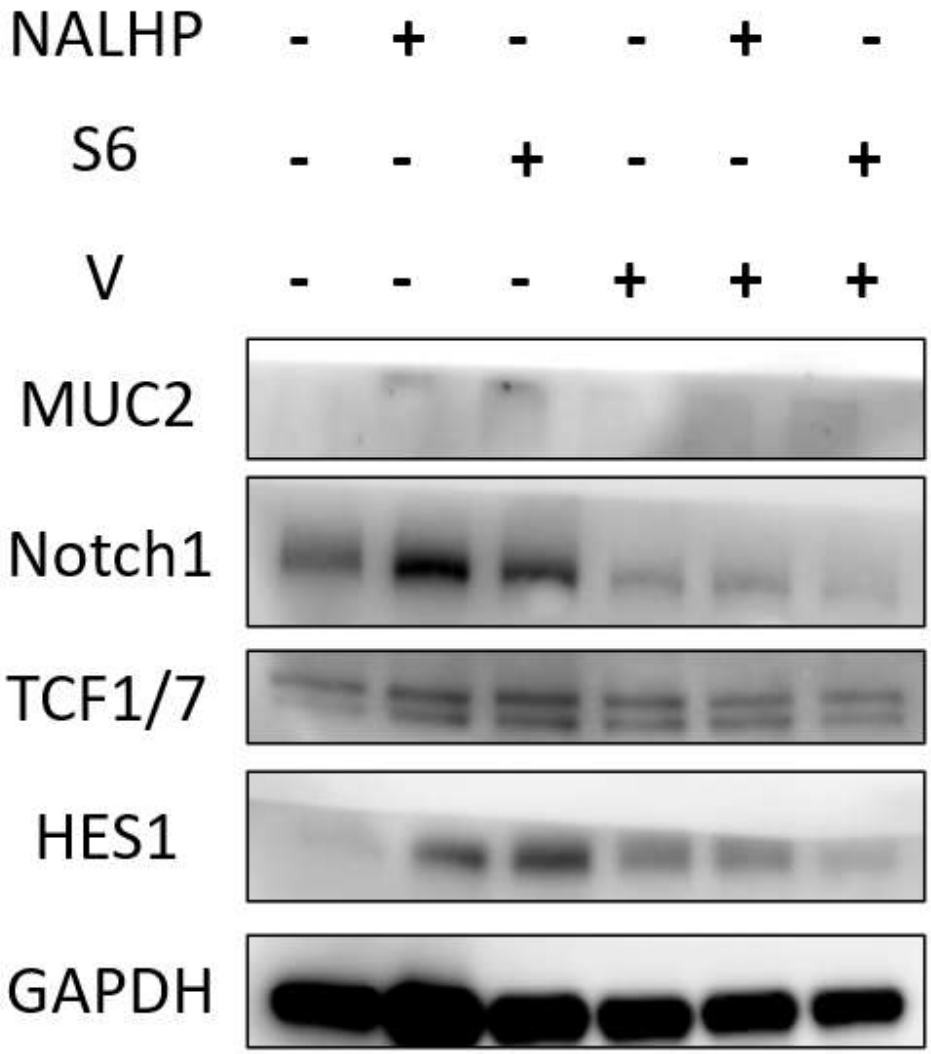

1206

1207

1208

Extended Data Fig.24 | Expression of key proteins after fondaparinux (Fonda) and non-anticoagulated fondaparinux (gs-Fonda) were co-cultured with UC organoids.

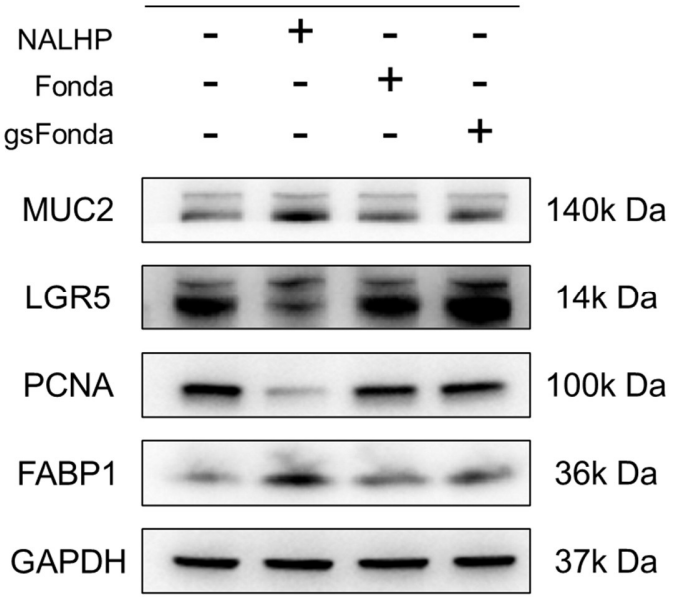

Extended Data is available for this paper.

Correspondence and requests for materials should be addressed to Xin-Hui Xing, Tel: 86-10-62794771, Email: xhxing@tsinghua.edu.cn, Yi Wang, Tel: 86-10-62773004, Email: wangyi671@mail.tsinghua.edu.cn, Xuan Jiang, Email: jiangxuan68@126.com